

Galaxy Formation and Evolution

Kentaro Nagamine^{1,2}  · Naveen Reddy³ · Emanuele Daddi⁴ · Mark T. Sargent⁵

Received: 12 December 2015 / Accepted: 13 June 2016 / Published online: 25 July 2016
© Springer Science+Business Media Dordrecht 2016

Abstract In this chapter, we discuss the current status of observational and computational studies on galaxy formation and evolution. In particular, a joint analysis of star-formation rates (SFRs), stellar masses, and metallicities of galaxies throughout cosmic time can shed light on the processes by which galaxies build up their stellar mass and enrich the environment with heavy elements. Comparison of such observations and the results of numerical simulations can give us insights on the physical importance of various feedback effects by supernovae and active galactic nuclei.

In Sect. 1, we first discuss the primary methods used to deduce the SFRs, stellar masses, and (primarily) gas-phase metallicities in high-redshift galaxies. Then, we show how these quantities are related to each other and evolve with time.

In Sect. 2, we further examine the distribution of SFRs in galaxies following the ‘Main Sequence’ paradigm. We show how the so-called ‘starbursts’ display higher specific SFRs and SF efficiencies by an order of magnitude. We use this to devise a simple description of the evolution of the star-forming galaxy population since $z \sim 3$ that can successfully

✉ K. Nagamine
kn@ess.sci.osaka-u.ac.jp

N. Reddy
naveenr@ucr.edu

E. Daddi
edaddi@cea.fr

- ¹ Theoretical Astrophysics, Department of Earth and Space Science, Graduate School of Science, Osaka University, 1-1 Machikaneyama, Toyonaka, Osaka 560-0043, Japan
- ² Department of Physics & Astronomy, University of Nevada, Las Vegas, 4505 S. Maryland Pkwy, Las Vegas, NV 89154-4002, USA
- ³ Department of Physics & Astronomy, University of California, Riverside, 900 University Avenue, Riverside, CA 92521, USA
- ⁴ CEA Saclay, DSM/Irfu/Sérvise d’Astrophysique, Orme des Merisiers, 91191 Gif-sur-Yvette Cedex, France
- ⁵ Astronomy Centre, Department of Physics and Astronomy, University of Sussex, Brighton BN1 9QH, UK

reproduce some of the observed statistics in the infrared (IR) wavelength. We also discuss the properties of molecular gas.

In Sect. 3, we highlight some of the recent studies of high-redshift galaxy formation using cosmological hydrodynamic simulations. We discuss the physical properties of simulated galaxies such as luminosity function and escape fraction of ionizing photons, which are important statistics for reionization of the Universe. In particular the escape fraction of ionizing photons has large uncertainties, and studying gamma-ray bursts (which is the main topic of this conference) can also set observational constraints on this uncertain physical parameter as well as cosmic star formation rate density.

Keywords Galaxies · Galaxy formation · Galaxy evolution · Star formation · Cosmology · Metallicity · Numerical simulations

1 Star-Forming Galaxies (SFGs): Linking Star-Formation Rate, Stellar Mass, Metallicity, and Their Evolution (Primary Author: N. Reddy)

A joint analysis of the star-formation rates (SFRs), stellar masses (M_*), and metallicities of galaxies throughout cosmic time can shed light on the processes by which galaxies build up their stellar mass, and enrich the interstellar and intergalactic media with heavy elements. In this chapter, we first discuss the primary methods used to deduce the SFRs, stellar masses, and (primarily) gas-phase metallicities in high-redshift galaxies. Then, we present a summary of how SFRs, stellar masses, and metallicities are related to each other, and how these relationships evolve with time. We conclude this section with future prospects of measuring these properties and their evolution.

The SFR, M_* , and metallicity (Z) are three of the fundamental characteristics of galaxies that we can use to discern how galaxies evolve with cosmic time. Partly spurred by the advent of large multi-wavelength datasets, there has been significant progress over the past couple of decades to infer the SFRs, stellar masses, and metallicities of galaxies across a large range in lookback time. This progress has, in turn, given us new insights into how galaxies form stars and build up their stellar mass, and how the heavy element content in the ISM of galaxies may vary with time depending on a number of factors. Nevertheless, a number of critical questions remain, some of which may be addressed with future astronomical facilities. In this section, we discuss the current state of our knowledge regarding the SFRs, stellar masses, and metallicities of high-redshift galaxies; how these properties relate to those we see in local galaxies; and we will highlight some of the challenges to fully incorporating these measurements into a coherent picture of galaxy formation.

1.1 Calculating SFR, M_* , and Metallicity

1.1.1 SFRs

A number of different multi-wavelength indicators may be used to estimate the SFRs of galaxies; some of the most common measures are summarized in Kennicutt (1998). The most frequently used indicator of star formation in *typical* star-forming galaxies (SFGs) at high redshift is the ultraviolet (UV) luminosity, as it is easily measured for distant galaxies. As the UV luminosity is susceptible to obscuration by interstellar dust, a correction must be applied to the UV luminosity. Typically, such corrections take advantage of the correlation between dustiness—as quantified by the ratio of the IR to UV luminosity, or essentially

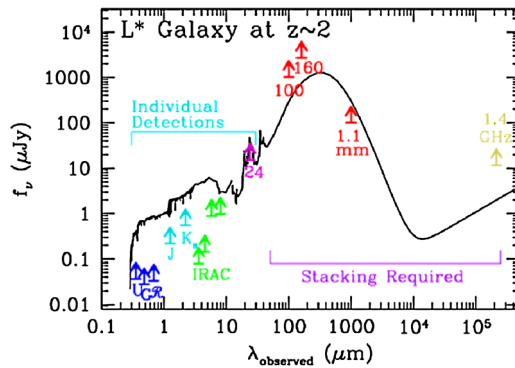


Fig. 1 Spectral energy distribution (SED) of a typical (L^*) galaxy at $z \sim 2$ (black), along with the detection limits of typical ground-based optical, near-IR, and IR imaging, and space-based mid-IR and far-IR imaging from *Spitzer* and *Herschel*, in the GOODS-North field. Also indicated is the detection limit of the VLA 1.4 GHz radio data in the GOODS-North field, as well as the detection limit for ALMA at 1.1 mm. Updated from Reddy et al. (2012a)

the dust-reprocessed light to that of the direct starlight—and the slope of the spectrum in the UV (Meurer et al. 1999). The wavelength dependence of dust obscuration implies that as the dustiness of a galaxy increases, the UV spectral slope becomes redder, as has been observed in local starburst galaxies (e.g., Meurer et al. 1999; Overzier et al. 2011), and subsequently the trends were shown for typical SFGs at $z \sim 2$ (e.g., Reddy et al. 2006; Daddi et al. 2007; Buat et al. 2012). The UV spectral slope is also sensitive to stellar population age, metallicity, and star-formation history (e.g., Kong et al. 2004; Seibert et al. 2005; Johnson et al. 2007; Dale et al. 2009; Reddy et al. 2010; Boquien et al. 2012; Wilkins et al. 2013), and so inferences of dustiness based on the UV slope must be viewed with caution, particularly for those galaxies where older stellar populations may contribute significantly to the near-UV flux of galaxies.

Ideally, one should obtain direct measurements of dust in high-redshift galaxies in order to more directly probe the amount of star formation in galaxies that may be obscured by dust. This may be accomplished by directly measuring dust emission in the mid- and far-infrared. While this technique can work well for the dustier and more luminous galaxies at high-redshift, current mid- and far-IR instrumentation (e.g., *Spitzer Space Telescope* and *Herschel Space Observatory*) are insufficiently sensitive to directly detect the dust emission from galaxies that are fainter than $\approx L_{\text{UV}}^*$ (e.g., Reddy et al. 2006; Fig. 1). To remedy this difficulty, analyses of the *average* mid- and far-IR emission have been carried out by “stacking” images for many galaxies (Reddy et al. 2006; Daddi et al. 2007; Reddy et al. 2012a), but this comes at the expense of losing information on the scatter in the dust emission from galaxy-to-galaxy. Nonetheless, *Spitzer*, *Herschel*, and ALMA observations have made a transformative impact on our understanding of the dust contents of the most luminous galaxies at high redshift (see review by Casey et al. 2014).

The limitations of the UV slope and direct far-IR measurements in probing dusty star-formation may be mitigated by the use of other SFR indicators. For instance, the radio 21 cm emission from SFGs is dominated by the synchrotron emission of electrons accelerated by supernovae, and provides an extinction-free indicator of SFR. Radio imaging is still insufficiently sensitive to directly detect typical star-forming galaxies at $z \gtrsim 1$, and also may suffer from significant contamination if there is an active galactic nucleus (AGN). While X-ray emission may be used as another extinction-free measure of SFR (Ranalli et al. 2003)

that can be measured for individual galaxies in deep Poisson-limited X-ray imaging, such emission may also vary with metallicity (Basu-Zych et al. 2013) and be affected by AGN.

The advent of multi-object near-infrared spectrographs (e.g., MOSFIRE, KMOS) have enabled measurements of the Balmer decrements ($H\alpha/H\beta$) of distant galaxies, as has been done locally for very large samples of galaxies (e.g., SDSS, Groves et al. 2012). For example, the recently commissioned MOSFIRE spectrograph on the Keck Telescope has been used to measure the Balmer decrements of a large sample of galaxies at $1.4 \leq z \leq 2.6$, enabling dust corrections to $H\alpha$ luminosities and dust-corrected estimates of the total SFR (Reddy et al. 2015). The Balmer lines provide the advantage of being less affected by SF history, as they arise only in the presence of hot, massive stars that can ionize hydrogen; and they can be measured now for individual galaxies without the need for spectral stacking (Reddy et al. 2015), as has been the case previously (e.g., Domínguez et al. 2013).

Finally, targeted observations with ALMA and other mm/sub-mm facilities, in combination with *Herschel* data, may be used to more accurately constrain dust temperature and mass and hence total infrared luminosities for more typical galaxies at high redshift. Similarly, gas masses measured with ALMA may also be used to estimate the amount of dust obscured star formation, albeit with large systematic uncertainties associated with the dust-to-gas ratio. More generally, resolved (kilo-parsec scale) imaging of the gas content (e.g., with IRAM or ALMA), combined with recombination line maps (e.g., made possible with the next generation of ground-based telescopes like TMT and ELT), will enable studies of the Kennicutt-Schmidt relation on resolved scales, thus clarifying the connection between gas surface density and SFR in high-redshift galaxies.

In the context of this conference, GRBs provide a unique avenue to constrain the shape of dust attenuation curve (e.g., Perley et al. 2013) which, in turn, will enable more accurate dust corrected SFRs. While each probe of SFR is subject to systematic uncertainties (e.g., such as the timescale for star formation, and the initial mass function), the use of multiple probes is generally indicated to provide the most robust measurement of SFRs of galaxies.

1.1.2 Stellar Masses

The primary method used to estimate stellar masses of distant galaxies is by fitting broadband photometry with stellar population synthesis models for different SF histories, ages, and reddenings. Commonly used empirical and theoretical models include Bruzual and Charlot (2003), Maraston (2005), Fioc and Rocca-Volmerange (1997), and Leitherer et al. (1999). Typically a grid of such models is computed assuming a range of SF histories (e.g., exponentially-declining, rising, constant, or bursty/stochastic), with a range of ages from the age of the Universe to some minimum value (e.g., in some cases this may be set to the dynamical timescale expected for the galaxy; Reddy et al. 2012b), and some range of reddening assuming a dust attenuation curve (e.g., Calzetti et al. 2000). Generally, stellar masses derived in this manner tend to have less *random* uncertainty than other parameters derived from such fitting, though the systematic uncertainty may be quite large. Sources of systematic uncertainty include the choice of IMF; the degree to which the most current episode of star formation dominates the optical light, commonly referred to as the “outshining” problem (Maraston 2005); and the contribution of thermally-pulsating AGBs to the rest-frame near-infrared light (e.g., Maraston 2005; Kriek et al. 2010).

The “SED-modeling” discussed above is usually performed using broadband photometry as typical SFGs at $z \gtrsim 1$ are too faint in the continuum for high signal-to-noise absorption spectroscopy to be feasible; the exception is for more massive galaxies at $z \sim 1$ where rest-optical continuum spectroscopy may be possible with longer integrations. Alternatively, one

can deduce the stellar mass, or at least provide a rough upper limit, if dynamical mass estimates are available. At high-redshift, these dynamical masses have been computed using either resolved observations of some gas-sensitive tracer, such as the CO emission, or by converting an H α luminosity to SFR, assuming a size, the Kennicutt-Schmidt relation, and a geometry for the galaxy (e.g., Erb et al. 2006b). Of course, while such measurements are subject to a number of systematic effects, they can in principle provide an independent handle on the stellar masses obtained from fitting the SEDs of galaxies.

1.1.3 Metallicities

Metallicities of high-redshift galaxies, specifically the *gas-phase* metallicities, are typically determined from strong-line abundance indicators that include some combination of the Balmer emission lines, and collisionally-excited forbidden oxygen and other weaker (e.g., [NII]) lines that arise from the ionized regions around massive stars. In rarer cases where a sufficiently high *S/N* and high spectral resolution spectrum has been obtained (e.g., for gravitationally lensed galaxies like cB58; Pettini et al. 2002), metallicities may be estimated from absorption lines either in the rest-UV (different sets of lines may be used to probe either the stellar metallicity, or the metal content of the ionized gas), or in the rest-optical (for stellar metallicities); see Shapley (2011) for a review of these metal indicators. Generally, direct electron temperature indicators which can be used to more robustly constrain the gas-phase metallicity are too weak to detect in individual high-redshift galaxy spectra, though access to these weaker features, like the [OIII]4363 line, will come with the next generation of large aperture telescopes (e.g., TMT, E-ELT, etc.).

There is a significant scatter and systematic offsets between different emission line indicators of metallicity (Kewley and Ellison 2008). Moreover, the application of locally-calibrated metallicity diagnostics to high-redshift galaxies may be inappropriate if the physical conditions (e.g., ionizing parameter, electron density) of the HII regions at high redshift differ from those found locally. Large rest-optical spectroscopic surveys of $z \gtrsim 1.4$ galaxies, made possible with multi-object near-IR spectrographs like MOSFIRE (McLean et al. 2012), have enabled the measurements of all the strong rest-optical emission lines for such galaxies. This, in turn, has enabled detailed assessments of the physical conditions in typical SFGs at high-redshift which underpin the metallicity measurements (e.g., Shapley et al. 2015).

1.2 The Relations Between SFR, M_* , and Metallicity, and Their Evolution

1.2.1 SFR– M_* Relation

The evolution of the relationship between SFR and M_* may be used to deduce, at least on average, how galaxies are building their stellar mass with cosmic time. Trends between SFR and M_* have been found at essentially all redshifts where the relationship has been probed, including at $z \lesssim 1$ (Noeske et al. 2007), and $z \gtrsim 2$ (Reddy et al. 2006; Daddi et al. 2007; Rodighiero et al. 2011; Whitaker et al. 2014). Generally, there is a universal trend for SFGs where the SFR increases with stellar mass, but with an increasing normalization with redshift (Fig. 2).

Generally, many studies have advocated that the scatter in the SFR– M_* relation is relatively “tight” (i.e., $\lesssim 0.3$ dex), however there are a number of reasons why the measured scatter should be considered as a lower limit. First, sample selection (e.g., in the UV) may be biased against detecting the highest SFR galaxies (and M_*) because they are very dusty, and

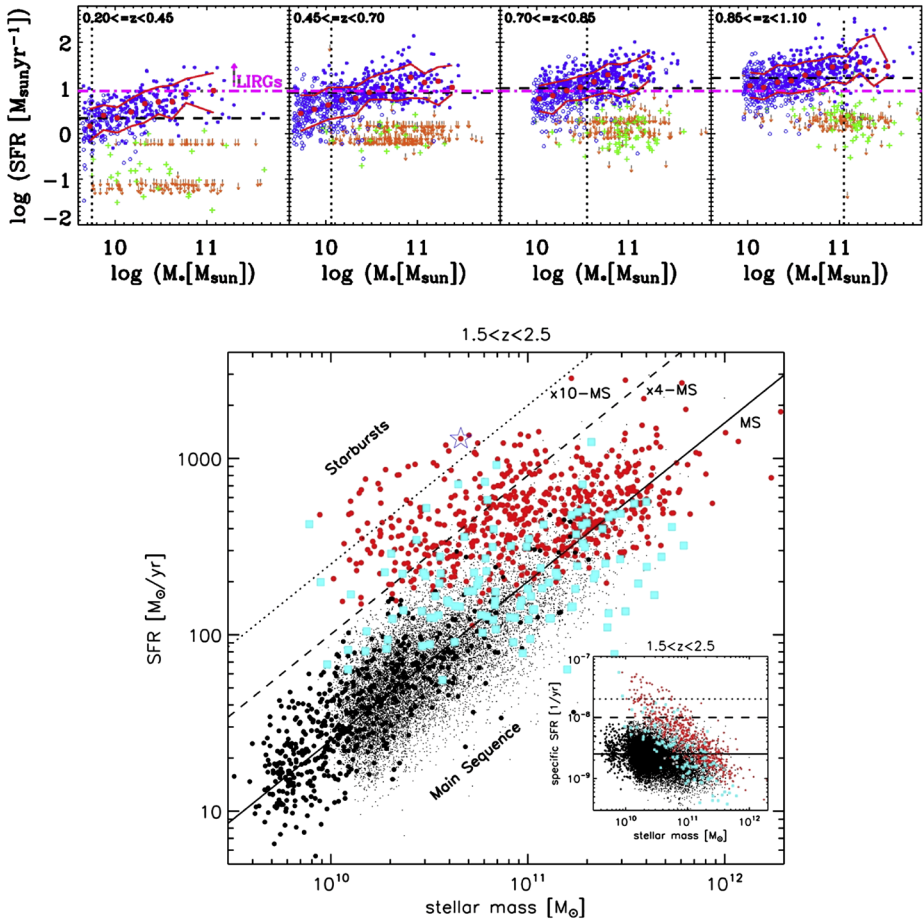


Fig. 2 *Top Row:* SFR vs. M_* for 2905 galaxies at $0.20 \lesssim z \lesssim 1.10$ from the AEGIS survey (from Noeske et al. 2007). *Bottom:* SFR vs. M_* for a sample of far-IR-detected (red and cyan points) and undetected (black points) galaxies at $z \sim 2$ (from Rodighiero et al. 2011)

thus one might underestimate the scatter in SFR at larger stellar masses (e.g., Daddi et al. 2007; Reddy et al. 2012b). On the other hand, while IR-selection may be more “complete” for the dustier and higher SFR galaxies, they will miss most of the typical SFGs. Further, when computing IR SFRs, one typically assumes a fixed conversion between IR luminosity and SFR. If this conversion changes from galaxy-to-galaxy, then the derived scatter in IR SFRs at a given M_* will be a lower limit to the true scatter. More generally, galaxy-to-galaxy variations in dust corrections, IMF, SF histories, etc., all imply that the scatter in the SFR– M_* relation, regardless of which SFR indicator is used, could be substantially larger than what has been claimed in the literature (Shivaei et al. 2015). Moreover, as many studies rely on photometric redshifts to derive stellar masses, and in some cases SFRs, the true scatter in SFR– M_* will be underestimated. In any case, the small scatter in the SFR– M_* relation has been interpreted as a reflection of the “smooth” manner in which galaxies build up their stellar mass (e.g. Davé 2008). However, given the uncertainties discussed above, we argue that the “scatter” derived for the SFR– M_* relation should be treated with caution.

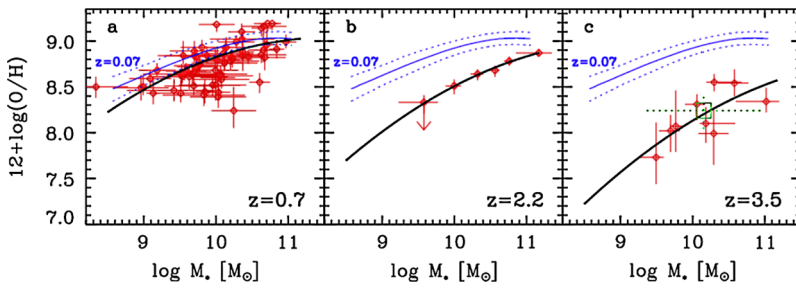


Fig. 3 Mass-metallicity relation at different redshifts, where the *blue solid and dotted lines* indicate the MZR at $z \sim 0.07$ from Kewley and Ellison (2008). Taken from Maiolino et al. (2008)

While the scatter may be difficult to pinpoint, the slope is generally more robust to the issues discussed above, except for that of sample selection and Malmquist bias where, for example, one is more prone to selecting galaxies with larger SFRs at a given low M_* for a flux- or line-selected (e.g. UV or $H\alpha$ selected) sample (Reddy et al. 2012b). While rest-optical selection can mitigate some of this Malmquist bias, such samples can still be incomplete especially if they rely on photometric redshifts which are generally poorly determined for young, low-mass, and essentially flat-spectrum galaxies. Nonetheless, significant efforts are focused on constraining the slope of the SFR– M_* relation at low masses, with the expectation that such galaxies may build up their stellar mass in a different way than their brighter counterparts (e.g., Whitaker et al. 2014), perhaps because different feedback processes, or the same feedback process with a different efficiency, operate in different mass regimes. Resolved SED modeling (e.g., with *Hubble Space Telescope*), as well as resolved imaging of the gas and dust contents in these galaxies may help to further clarify the relationship between stellar populations, gas content, and feedback.

1.2.2 Mass–Metallicity Relation

Like the SFR– M_* relation, the mass–metallicity relation (MZR) has been found across a wide swath of redshift, at $z \sim 0$ (Tremonti et al. 2004), $z \sim 0.7$ (Savaglio et al. 2005), $z \sim 2.3$ (Erb et al. 2006a), and $z \gtrsim 3$ (Maiolino et al. 2008); see Fig. 3. These studies indicate that high-redshift galaxies are less metal-rich than local galaxies at a given stellar mass. To infer this evolution, however, previous studies had to rely on comparisons of the MZR that used different metallicity indicators at different redshifts (thus introducing some uncertainty in the evolution owing to systematic differences in metallicity indicators), and made the assumption that the local calibrations between strong-line emission indicators and the oxygen abundance apply at all redshifts.

What has been lacking previously is access to the same metallicity indicator at different redshifts, as well as an understanding of how such indicators scale with oxygen abundance at different redshifts. Recent advances in near-IR detector technology (e.g., MOSFIRE, KMOS) have begun to remedy this situation. For example, the MOSFIRE instrument enables access to the same strong rest-optical emission lines, including [OII], [OIII], $H\beta$ and $H\alpha$, at high redshift ($1.4 \lesssim z \lesssim 2.6$) that are used to estimate metallicities in local galaxies. Further, the sensitivity of these observations is sufficient to obtain metallicity estimates for individual objects rather than for an ensemble (Fig. 4).

Surveys like MOSDEF, which is sensitive to a number of different strong rest-optical emission lines for $1.4 \lesssim z \lesssim 3.8$ galaxies, can enable detailed photoionization modeling to

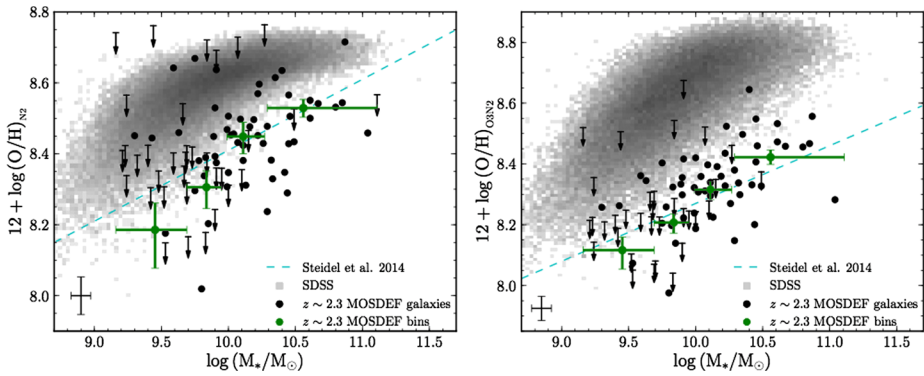


Fig. 4 Mass-metallicity relation at $z \sim 2.3$ based on data from the MOSFIRE Deep Evolution Field (MOSDEF) survey. Gas-phase metallicities are calculated using both the N2 (*left*) and O3N2 (*right*) indices, where upper limits are indicated by the *arrows*. Taken from Sanders et al. (2015)

jointly constrain the electron densities, ionizing parameters and hardness, and metallicities, of high-redshift galaxies. For example, preliminary studies suggest that for at a fixed ionization parameter, the high-redshift galaxies have the same metallicities as those of local galaxies (Shapley et al. 2015). Furthermore, these studies have suggested that high-redshift galaxies are more abundant in nitrogen at a given gas-phase metallicity relative to their local counterparts, perhaps due to the properties of massive stellar populations at high redshift (Masters et al. 2014; Shapley et al. 2015). Regardless, these larger samples will enable more detailed comparisons of the slope and scatter of the MZR relation to the predictions of galaxy simulations in order to deduce the effect of gas inflows and outflows on the metal content and SFRs of galaxies across cosmic time (e.g., Finlator and Davé 2008).

1.3 Connections Between SFR, M_* , and Metallicity, and Future Directions

To first order, the stellar mass simply reflects the integral of the SFR with time (modulo the fraction of gas that is returned to the ISM). Similarly, the metallicity reflects the heavy element yield from this star formation. These connections motivated Mannucci et al. (2010) to propose a model whereby the SFRs, M_* , and metallicities of galaxies lie on a “fundamental plane” (or “fundamental metallicity relation”, FMR) that does not evolve, and that the observed redshift evolution of the MZR simply reflects that change in average SFRs probed at each redshift. However, more recent studies (e.g., Steidel et al. 2014; Troncoso et al. 2014; Sanders et al. 2015) suggest that high-redshift galaxies do not fall on the FMR defined by local galaxies. Current and forthcoming large surveys will enable detailed photo-ionization modeling and more robust estimates of the gas-phase metallicities over a large swath of cosmic time. This, in turn, should give us a better indication of the effects of gas inflows and outflows on the evolution of galaxies.

Aside from this impending improvement in our knowledge of the joint relationship between the SFRs, M_* , and metallicities, future facilities and instruments will undoubtedly provide a more “resolved” picture of these relationships. Multi-object spectrographs on $\gtrsim 30$ m class telescopes will enable the measurement of weaker lines like [OIII] $\lambda 4363$, giving us a direct metallicity indicator with which to calibrate all the strong line indicators. These facilities will also extend upon the currently known trends and scatter in the SFR– M_* and MZR relations to fainter galaxies that host the bulk of the star formation activity at high redshift (Reddy and Steidel 2009; Bouwens et al. 2015).

Combined with adaptive optics, the future ground-based facilities will enable a study of the connection between SFR, M_* , and metallicity on kilo-parsec scales where the effects of galaxy feedback may be modeled more easily. Finally, we note that the *James Webb Space Telescope* will access the strong line indicators discussed above for galaxies at even higher redshifts (up to $z \sim 6$) where galaxies are evolving on more rapid timescales.

Probing faint galaxies at high redshift with gamma-ray bursts (GRBs), the topic of this conference, provides an alternative and complementary means of evaluating the connections between SFR, stellar mass, and metallicity. In particular, because of their stellar origin, GRBs can be found in very faint galaxies that would otherwise be “missed” in current surveys. Aside from opening up a new parameter space, GRBs also offer the opportunity to measure stellar metallicities using rest-UV lines (e.g., CIV; Berger et al. 2006; Sparre et al. 2014), or traditional metallicity diagnostics for DLAs that correspond to GRB host galaxies (Ledoux et al. 2009; Cucchiara et al. 2015). Understanding the context of GRB hosts in terms of the previously studied galaxy populations will require a more quantitative connection between the propensity for GRBs and host galaxy properties.

2 Global Properties of SFGs at $z < 4$ (Primary Author: E. Daddi & M.T. Sargent)

In this section, we further discuss modern understanding of the distribution of SFRs in galaxies following the Main Sequence paradigm. While the majority of SFGs are observed to be close to the relation between SFR and M_* , a smaller subset of the population—so-called ‘starbursts’—display specific SFRs and SF efficiencies that exceed those of normal (main-sequence) galaxies by up to an order of magnitude. This can be used to devise a simple description of the evolution of the star-forming galaxy population since $z \sim 3$ that can successfully reproduce the shape of the IR luminosity function of galaxies as a function of redshift, the IR number counts and Planck-Herschel power spectrum of the cosmic IR background, i.e., clustering of star formation. The evolution of star formation in galaxies is linked to the underlying properties of the molecular gas. Typical Main Sequence galaxies have warmer gas temperatures at high redshifts and display relatively stronger high-J CO emission, probably linked to their clumpier interstellar medium. Evolution at even higher redshifts is currently under investigation. A key driver is the expected decrease of metallicities towards early times.

At high and low redshift, the population of SFGs comprise a mix of (1) ‘normal’ SFGs following a narrow relation—the ‘star-forming main sequence’—between SFR and M_* (e.g., Brinchmann et al. 2004; Salmi et al. 2012), and (2) ‘starbursts’ with a large excess specific SFR (sSFR) compared to typical objects on the SFR– M_* main sequence.

Investigations on the nature of the star-forming population have advanced our understanding by characterizing the systematic differences between starburst and normal galaxies while also revealing large homogeneity within each of these populations, at fixed redshift and also as a function of redshift: starburst galaxies tend to be more compact (e.g., Elbaz et al. 2011; Rujopakarn et al. 2011) than main-sequence galaxies. The latter show a stellar morphology that is well-fitted by exponential disks (e.g. Wuyts et al. 2011) (as opposed to high Sersic- n for the spheroids), they display IR line deficits (e.g., PAHs or in the far-IR the [CII]-line; Elbaz et al. 2011; Graciá-Carpio et al. 2011), both of which are consistent with a scenario in which very compact, more efficient star formation is taking place, in line with the up to tenfold higher SF efficiency (SFE) reported by molecular gas observations of distant SFGs (e.g. Daddi et al. 2010b; Genzel et al. 2010).

In the next sections we will show that a very simple characterization of the evolution of SFGs based on these two populations can account for a large variety of observables in galaxy formation and evolution, without the need of fine tuning or external parameters. Such a simple and self-consistent scheme (referred to as the ‘Two Star-Formation Mode framework’; 2-SFM) allows one to predict basic properties of SFGs, like the IR luminosity function (LF), IR source counts, clustering, or molecular gas mass functions, starting from basic observables (e.g., the evolution of sSFR for main-sequence galaxies and stellar mass functions) and observed correlations (e.g., the main sequence or the integrated Kennicutt-Schmidt law connecting their gas content and SFR).

2.1 IR Properties of SFGs: Luminosity Functions, Source Counts and IR Clustering

Widely used, basic characterization of galaxy populations are the mass functions (MFs) and LFs. While the former is generally well reproduced by a Schechter function (e.g., Ilbert et al. 2010), the IR LF (i.e., the distribution of SFRs) is not, requiring for example double power law or exponentials (e.g., Le Flocc’h et al. 2005; Magnelli et al. 2009). When accounting for the two SF modes among SFGs (bursty versus main sequence SF), this difference is naturally explained, suggesting that from the evolution of stellar mass and IR LFs, one can gather information on the interplay among the two SF modes at different redshifts. In the following we show how the contribution of main-sequence and starburst galaxies to IR LFs (hence to the SFR density) can be disentangled. We use this information to infer source counts from 24 to 1100 μm and predict the distribution of star formation among dark matter halos as a function of redshift.

2.1.1 IR LF at $z < 2.5$

The main sequence evolution with redshift out to $z \sim 2$ (e.g. Elbaz et al. 2011; Karim et al. 2011) and the evolution of galaxy stellar MFs to similar redshifts are well characterized, and can be jointly used to derive the IR LF evolution if the distribution of sSFR at fixed stellar mass is available. We use the results of Rodighiero et al. (2011) for SFGs at $z \sim 2$, decomposed into two log-normal components (see Fig. 5, left, corresponding to main-sequence and—likely interaction-induced—starburst-like SF activity, respectively; see Sargent et al. 2012 for more details and discussion of the underlying assumptions). The conversion of stellar MFs to IR LF is effectively a convolution of the MF and an evolutionary double-Gaussian kernel with (i) normalization fixed by the shape of the MF, and (ii) main-sequence peak position that—given the redshift—is uniquely determined by the position of the SF main sequence in the (s)SFR vs. M_* plane. As a result of this approach, we can distinguish the individual contribution to the IR LF of main sequence versus bursty SF (see Fig. 5, right).

Figure 1 shows that the stellar MF and the IR LF (i.e., the SFR distribution) of SFGs at $z \leq 2$ evolve consistently (see also Bell et al. 2007). The bright end of the IR LFs is entirely determined by starburst galaxies. These results imply that the contribution of starbursts to the cosmic SFR density is (8–14 %) perhaps marginally increasing with redshift at $z < 2$. We can account for the well-known observation that most ULIRGs at $z = 0$ are starbursts (e.g., Sanders and Mirabel 1996). Instead, the majority of ULIRGs at $z > 0.9$ live on the main-sequence. In fact, their high SFR ($> 100 M_{\odot}/\text{yr}$) is not thought to be triggered by merging as in most local ULIRGs but is the result of large gas reservoirs in high-redshift disks (e.g., Daddi et al. 2010a; Tacconi et al. 2010; Geach et al. 2011). Local and distant ULIRGs are intrinsically different objects, in this respect, despite having similar SFRs by definition.

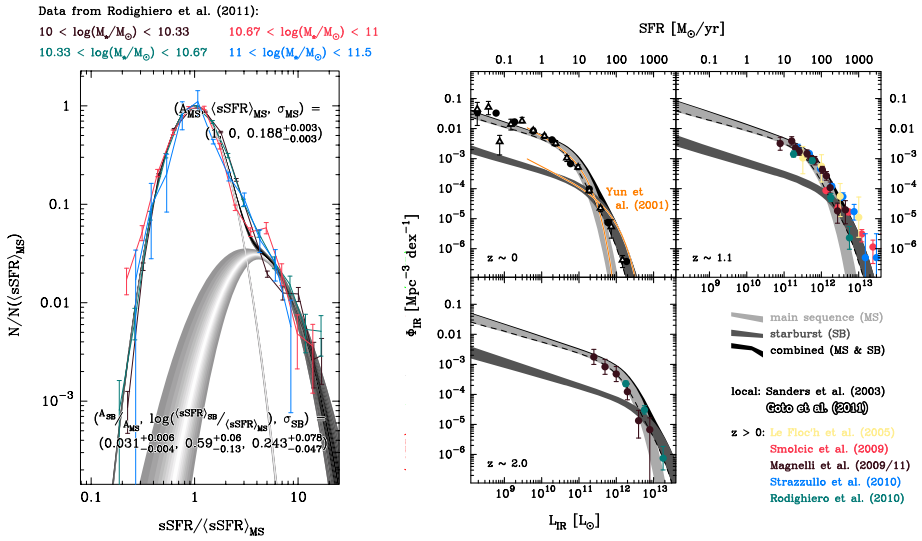


Fig. 5 *Left*: Distributions of sSFR are self-similar in mass bins (for $M_*/M_\odot > 10^{10}$ from Rodighiero et al. 2011) and can be decomposed into two log-normal components, one accounting for the distribution of main-sequence galaxies, the other enhanced (s)SFRs with starburstiness (likely due to interactions, affecting the galaxies at various degrees). *Right*: Contribution to the IR LFs (or equivalently, SFR distributions Kennicutt (1998)), resulting from normal (light grey) and burst-like (dark grey) galaxies. Literature measurements are displayed in color; see legend

2.1.2 IR Source Counts

An additional important observable on which evolutionary models of SFGs should be tested are IR number counts over a variety of multi-wavelength bands. Purely semi-analytical models (e.g., Lacey et al. 2010) have difficulties reproducing IR number counts, while phenomenological or hybrid models (e.g., Béthermin et al. 2011; Gruppioni et al. 2011) reach better results but are in general forced to adopt ad-hoc parameters to force agreement in the fit and thus imply evolution of the IR LFs which are not necessarily physically motivated. The 2-SFM framework introduced in Sect. 2.1.1 can be used to naturally predict IR galaxy counts.

In our framework we can assign SFRs (hence bolometric IR luminosities) to galaxies as a function of redshift. The main additional ingredient to predict their observed fluxes is determining their SED. We have been measuring the evolution of the average SED of galaxies through redshift (Magdis et al. 2012b) which motivate adopting a very simple SED library of templates: a single SED for both main sequence and starburst galaxies at fixed redshift but with both rising in dust temperature with rising redshift. The predictions of such a simple model agree nicely with measurements of differential galaxy counts from 24 μ m to 1.4 GHz in Fig. 6. Overall, the observations of galaxy counts are well reproduced, showing the effectiveness of the key ingredient of the 2-SFM approach, which is the explicit distinction between normal and starbursting galaxies. When distinguishing main-sequence from bursty galaxies we can investigate which selection biases could be present toward normal or starburst galaxies in surveys defined at a variety of wavelengths and flux depth levels. Given the overall paucity of starbursts, it is main-sequence galaxies that dominate number counts, basically independently on flux densities and wavelengths. Nevertheless,

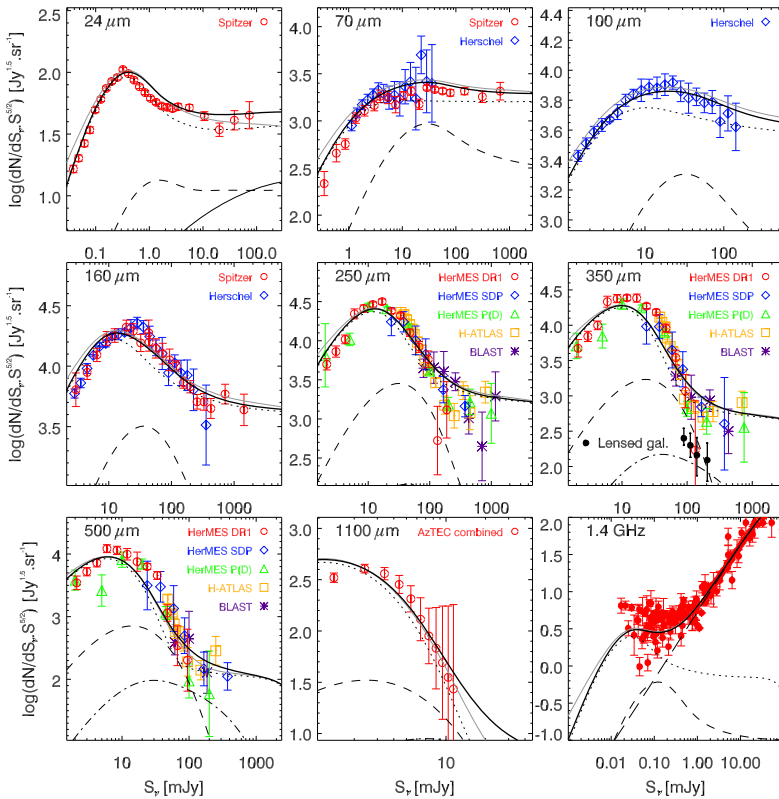


Fig. 6 24 μm to 1.4 GHz number counts (reproduced from Béthermin et al. 2012b). *Solid line*—total counts predicted by the 2-SFM framework, including a contribution for AGN-emission, mass-dependent dust attenuation and lensed sources; *gray line*—counts predicted when neglecting the three aforementioned refinements; *dotted line*—main-sequence contribution; *short-dashed line*—starburst contribution; *dot-dashed line*—lensed sources; *triple-dot-dashed line*—difference between counts with and without AGN contribution. At 1.4 GHz the model for SFGs was combined with the model of AGN-driven radio sources by Massardi et al. (2010; *long-dashed line*). Despite some deviance, e.g. at the faint end in some cases, this is a high successful reproduction of the observations given precedent literature and the lack of adjustable parameters

their overall importance can vary substantially and becomes quite relevant ($\sim 30\%$) around 30 mJy at 70 μm and 50 mJy at 350 and 500 μm .

Despite its simplicity and the lack of adjustable parameters, these 2-SFM predictions result in one of the best reproduction achieved so far to IR source counts, including counts per redshift slice at SPIRE wavelengths, which were poorly reproduced in earlier models.

2.1.3 Star Formation and Dark Matter Halos

This simple framework can be extended further, using observations of how stellar masses and dark matter masses are connected via measurements of clustering (e.g., Béthermin et al. 2014) and/or abundance matching techniques (e.g., Behroozi et al. 2013). This allows one in turn to distribute star formation among dark matter halos, without the need of further external parameter or tunings. Béthermin et al. (2013) showed that this approach successfully predicts the (cross-)power spectra of the cosmic infrared background (CIB), the cross-

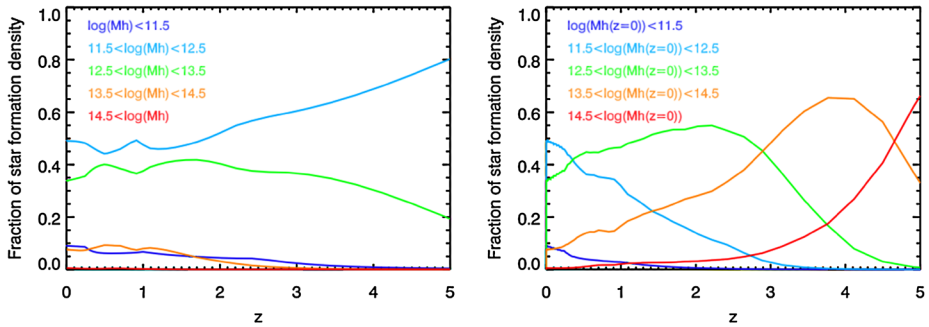


Fig. 7 Both panels show the fraction of SFR density as distributed among dark matter halos as a function of redshift, but considering the instantaneous dark matter mass at each redshift (*left*) or the halo mass where the activity will end up at $z = 0$ (*right*) (from Béthermin et al. 2013)

correlation between CIB and cosmic microwave background (CMB) lensing, and the correlation functions of bright, resolved infrared galaxies measured by Herschel, Planck, ACT, and SPT. This is an important result as it shows that we have a good basic understanding on how to associate activity to hosting dark matter halos, at least for typical structures (most activity in all redshifts is happening inside $11.5 < \log M_{\text{DM}} < 13.5$ halos; Fig. 7). At the same time, given the well understood evolutionary behavior of dark matter halos with time, this approach can be used to investigate in which kind of dark matter halos at $z = 0$ will eventually end-up the SFR activity observed in the distant Universe (Fig. 7): this is typically borderline clusters with $10^{14} M_{\odot}$ $z = 0$ halos for $3 < z < 4.5$ activity, and $10^{13} M_{\odot}$ $z = 0$ small groups at $1 < z < 3$.

2.2 Molecular Gas in SFGs Near and Far

The evolution of molecular gas reservoirs in galaxies, including normal and starburst cases, can also be described in the powerful framework we have been sketching so far, based on the well determined evolution of the stellar MF at $z < 2.5$ and on the distribution of sSFR with naturally decomposes into normal and burst like modes (at fixed stellar mass, and invariantly to first order with redshifts and stellar mass). Similarly to what done for IR source counts in Sect. 2.1.2, we can attribute gas masses to galaxies based on their IR luminosity once they are classified into main sequence and starburst objects. The choice of the SFE is based on the different observational behavior of normal versus starburst galaxies (Sect. 2.2.1). We apply these relations to galaxy populations in the 2-SFM framework to show that the coherent increase of gas fraction (f_{gas}) in normal galaxies to high redshift is driving the evolution of the main sequence to $z \sim 3$.

2.2.1 Gas Reservoirs in SFGs: Basic Scaling Relations

Roughly 50–100 galaxies at $z > 0.4$ selected to be on the main sequence have been followed-up in CO in recent years (e.g. Daddi et al. 2010a; Genzel et al. 2010; Tacconi et al. 2010; Geach et al. 2011; Tacconi et al. 2013), providing information on their molecular gas properties. We combine this high- z literature data with a roughly equally sized local sample—including massive galaxies from the HERACLES survey (Leroy et al. 2009) and AKARI-detected disks from the COLD GASS survey (Saintonge et al. 2011)—and plot their L_{IR} and CO-luminosity L'_{CO} in Fig. 8(left). The well-defined correlation between these observational

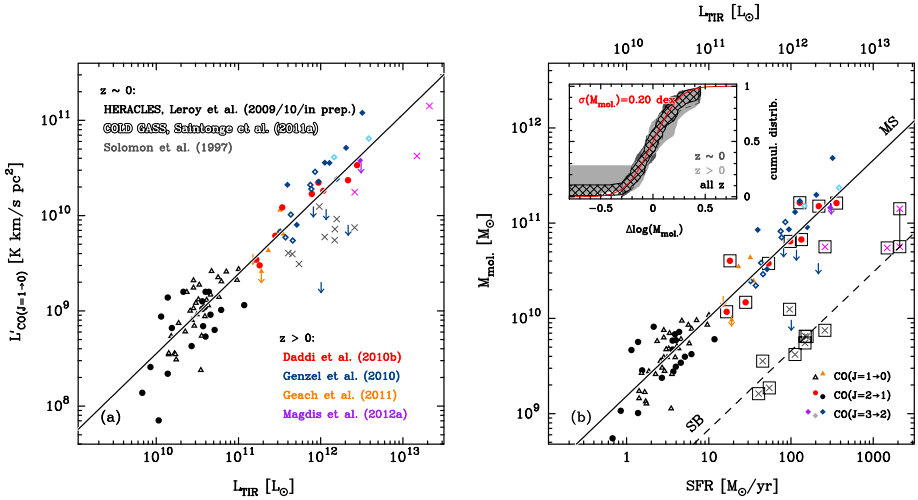


Fig. 8 Correlation between measures of SFR and gas content for massive ($M_{*} > 10^{10} M_{\odot}$), main-sequence galaxies in the nearby universe and at $z > 0.4$ (see legends in panel (a) for data source). Selected starburst galaxies with measured conversion factors α_{CO} from Solomon et al. (1997) and Magdis et al. (2012b) are plotted with crosses. (a): Correlation between infrared luminosity (L_{IR}) and CO(1 \rightarrow 0) luminosity ($L'_{CO(1-0)}$; standard excitations corrections—e.g. Dannerbauer et al. (2009), Leroy et al. (2009)—were applied to $J > 1$ transitions, cf. legend in panel (b)) with best-fitting relation derived for the main-sequence galaxy sample overplotted in black. (b): Correlation between SFR and molecular gas mass ($M_{mol.}$), the latter having been derived based on either (a) observational determinations of α_{CO} (available for sources with boxed symbols) or (b) using a metallicity-dependent conversion factor (see text). The dispersion about the best-fit linear trend (solid black line) for main-sequence galaxies is approximately Gaussian with a dispersion $\sigma(M_{mol.}) \sim 0.2$ dex (red curve in inset). Dashed line—offset locus with approx. 15-fold higher SFE for strong starburst galaxies

proxies of SFR and molecular gas mass suggests that there is a high degree of homogeneity between low- and high-redshift main-sequence galaxies in terms of their molecular gas properties. We measure a dispersion of 0.2 dex in the correlation between molecular gas mass $M_{mol.}$ and SFR (see Fig. 8, right), where we have applied either (a) observational determinations of α_{CO} (available for sources with boxed symbols) or (b) a metallicity-dependent conversion factor¹ to convert CO-luminosities to molecular gas masses. The best-fit, inverse integrated Kennicutt-Schmidt (K-S) relation plotted in Fig. 8 is slightly sublinear ($M_{mol.} \propto SFR^{\beta_{K-S}}$, with $\beta_{K-S} = 0.83$), but due to the small overlap in luminosity-space between local and $z > 0$ main-sequence galaxies a redshift-dependent integrated K-S relation with different slope and changing normalization currently cannot be excluded. Note, however, that by considering stacked samples of $z \sim 0$ and 2 main-sequence galaxies from Magdis et al. (2012b)—who inferred molecular gas masses indirectly by measuring of average dust masses—the correlation is found to extend over at least two orders of (partially) overlapping magnitude in SFR at both redshifts, suggesting that the integrated K-S relation

¹Recent observational studies, as well as a numerical predictions on a metallicity-dependence of the conversion factor parametrized as $\alpha_{CO} \propto Z^{\gamma}$ find a broad range of power-law exponents γ ranging from -0.5 to -2 (e.g. Feldmann et al. 2012; Genzel et al. 2012; Schruba et al. 2012). Here we adopt an intermediate value of the exponent, $\gamma \simeq -0.9$, which results in the best fit to the $z \sim 0$ CO LF by Keres et al. (2003) (see Fig. 10) within the 2-SFM framework and its underlying assumptions (see Sargent et al. 2014).

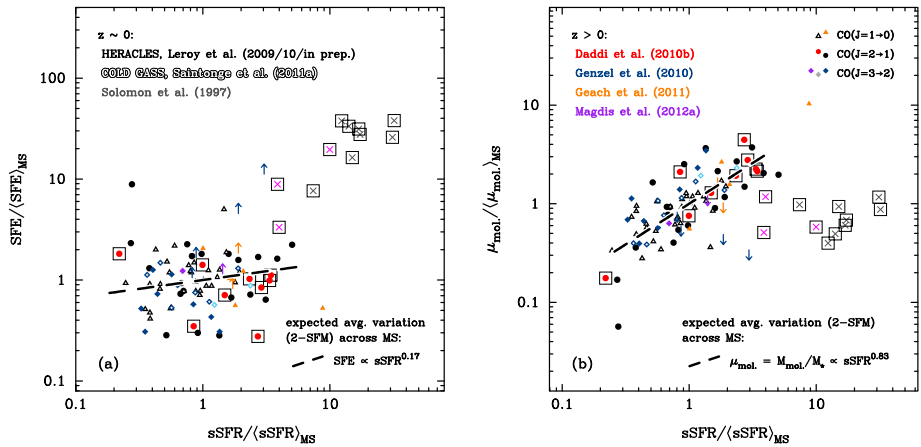


Fig. 9 Star-formation efficiency (*left*), and molecular gas mass fraction, $\mu_{\text{mol}} \equiv M_{\text{mol}}/M_{\star}$ (*right*) vs. sSFR for selected main-sequence galaxies and starbursts at $z < 3$ (all measurements normalized to the M_{\star} - and redshift-dependent average of the main-sequence and all symbols and data as in Fig. 8). When normalized to the characteristic main-sequence value, the homogeneous behavior of main-sequence galaxies at all redshifts becomes visible: SFE varies very little within the main sequence while f_{gas} steadily rises. Starbursting sources, on the other hand, have a gas content that is similar to the average main-sequence galaxy but display enhanced SFEs that lead to their excess (s)SFR

to first order is a universal function of redshift for massive, normal SFGs ($M_{\star}/M_{\odot} > 10^{10}$) at $z < 3$.

To further highlight this uniform behavior across a broad range of redshift, in Fig. 9 we plot SFE and gas fractions that have been normalized to the (mass- and redshift-dependent) average values of a galaxy located directly on the main-sequence and compare these to the analogously normalized sSFR (i.e. the offset from the main sequence). This representation of the data reveals that: (1) at all redshifts, the SFE in main-sequence galaxies in our “calibration sample” is almost independent of their position within the main sequence, while their SFR rises in lockstep with f_{gas} ; (2) starburst galaxies (here we consider a small sample of local and high- z starbursts with measured α_{CO}) have similarly-sized gas reservoirs as normal galaxies but are characterized by a strongly enhanced SFE. The dashed line in Fig. 9 illustrates the expected variation of SFE ($\propto \text{sSFR}^{-0.17}$) and f_{gas} ($\propto \text{sSFR}^{0.83}$) within the main sequence as it follows from the best-fit integrated K-S relation shown in Fig. 8(b), in agreement with the dust mass-based findings of Magdis et al. (2012b).

2.2.2 Redshift Evolution of Gas Fractions

Given the tight correlations between M_{\star} and SFR, and between SFR and H_2 -mass, it is straightforward to model the evolution of f_{gas} in main sequence galaxies where $M_{\text{gas}}/M_{\star} \equiv \text{const.} \times \text{SFR}(M_{\star})^{\beta_{\text{K-S}}}/M_{\star}$. This results in predictions for gas fractions in main sequence galaxies at $z < 3$ in good agreement with observations (Magdis et al. 2012a) confirming that the gas content of secularly-evolving SFGs is an important driver of the cosmic sSFR-evolution. This is consistent with the observation in Fig. 9 that, also at fixed redshift, variations of sSFR across the main sequence are driven by varying f_{gas} . Of course, all this agreement is also, in part, by construction. It would considerably worsen if the various means by which total molecular masses are estimated were to be incorrect, which would be surprising given the overall consistency from CO, dust and dynamical estimations.

2.2.3 Molecular Gas Mass Functions and the Molecular Gas History of the Universe

To estimate the redshift evolution of the distribution of molecular gas masses in normal galaxies we convert the main-sequence component of the SFR-distribution depicted in Fig. 5 to a gas mass distribution by means of the best-fitting integrated K-S relation of Fig. 8(b). For the starbursting population we assume that the SFE increase (with respect to the value of the main-sequence state prior to the onset of burst activity) in these systems scales with the boost in star-formation rate engendered by the burst (see Sargent et al. 2012 for details). This kind of behavior is suggested by the roughly similar excess in sSFR and SFE observed in Fig. 9(a) and also seen in numerical simulations of galaxy mergers (e.g. Di Matteo et al. 2007). The total molecular gas MF (i.e. including both normal and starburst galaxies) inferred using this approach for the SFG population at $z \sim 0, 2$ & 5 is shown in Fig. 10. Note that the H_2 -MF is only observationally constrained in the local universe (Keres et al. 2003; Obreschkow and Rawlings 2009a) where the measurements are entirely consistent with the 2-SFM predictions. (This is also true of the predicted CO LFs—cf. Fig. 10—which follow from the H_2 -MFs after (a) assigning to main-sequence galaxies α_{CO} -values based on statistically-derived metallicities, computed using the fundamental metallicity relation of Mannucci et al. (2010) given the known SFR and M_* , and (b) for starbursts assumes a conversion factor that scales inversely with the SFE-enhancement. (See Sargent et al. 2014 for additional details and underlying assumptions/simplifications.) The dominant contribution to the predicted H_2 -MF stems from main-sequence galaxies which hence also are the main contributors to the evolution of the cosmic abundance of molecular gas which is obtained by integration of the molecular gas mass functions and which is shown in Fig. 11. This indirect measurement of the comoving H_2 -density reveals a roughly 5-fold increase of the molecular content of the Universe out to $z \sim 1.5$ where it roughly equals the stellar mass density and the cosmic abundance of atomic hydrogen. The increase traces the rise of the cosmic SFRD but is roughly five times smaller due to the sublinear relation between SFR and H_2 -mass found in Fig. 8 which implies slowly rising SFEs for the typical SFGs (of stellar mass $\sim 5 \times 10^{10} M_{\odot}$, cf. Karim et al. 2011) that contribute most to the cosmic SFRD density over this time. Overall, there is a large range of predictions from alternative models at high redshifts (Fig. 10, emphasizing the need for observations to confirm our results based on scaling relations).

2.2.4 Evolution of the Interstellar Medium

While there are no convincing evidence yet that star formation laws are changing with redshift, the strong rise of the specific SFR of galaxies appears to be accompanied by substantial changes in the properties of the interstellar medium of Main Sequence galaxies, other than a simple augmentation of the gas reservoirs. This is manifested already in evolution in optical emission line ratios (e.g., Steidel et al. 2014), which requires variations in the radiation field that the gas is witnessing. From the point of view of the ISM, several studies now have converged to show that this evolution is paralleled for Main Sequence galaxies to a rise in the intensity of the radiation field which is heating dust (the parameter $\langle U \rangle$ scaling like $(1+z)^{1.2-1.8}$; Magdis et al. 2012b; Béthermin et al. 2015; Genzel et al. 2015). This is understood to be driven by a combination of rising star formation efficiencies and declining metallicities towards high- z (at fixed stellar mass; Magdis et al. 2012a, 2012b). On a similar manner, observations of CO excitation for Main Sequence galaxies also show evolution from low redshift disk-like SFGs. In particular, high- z galaxies have much stronger CO[5-4] transitions, which points to a higher relevance of denser and/or warmer gas (Daddi et al.

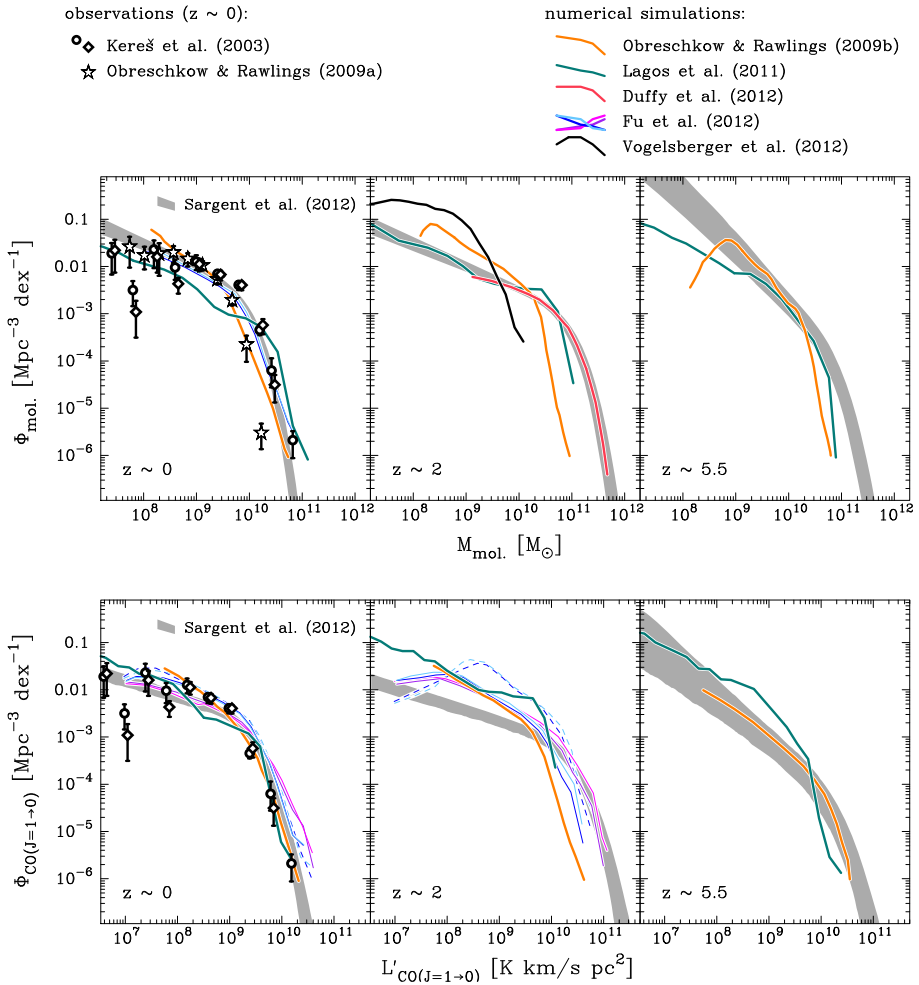


Fig. 10 Molecular gas MFs (*upper row*; grey shading) and CO(1-0) LFs (*lower row*) based on (1) the evolution of the stellar MF of SFGs, (2) the redshift evolution of the sSFR of main-sequence galaxies, (3) the distribution of main-sequence and starbursting galaxies in the SFR- M_* -plane (see Fig. 5, left) and (4) a metallicity-dependent conversion factor α_{CO} . MFs/LFs include contributions both from ‘secular’ and burst-like star formation (the latter being characterized by increased SFEs with respect to the secular mode which is assumed to be typical of galaxies residing on the main sequence). *Colored lines*—predictions of recent semi-analytical models (see *legend* above figure) covering a similar redshift range as the empirically-motivated, predictive analysis of Sargent et al. (2014). At $z \sim 0$ we show observational constraints on the local MF/LF reported in Keres et al. (2003) and Obreschkow and Rawlings (2009b)

2015; Fig. 12). Empirically the high-J to low-J CO ratios among various populations is well correlated to their radiation field intensity $\langle U \rangle$ (hence dust temperature) as well as to star formation surface brightness (hence gas density). Simulations suggest that such a dense/warm gas is typically associated to clumpy star-forming regions (Bournaud et al. 2015). This is supported by observations but not fully proven yet, and there is debate on the real mass and relevance of clumpy star formation in the distant Universe. However, a massive clump formation event has recently been observed (Zanella et al. 2015).

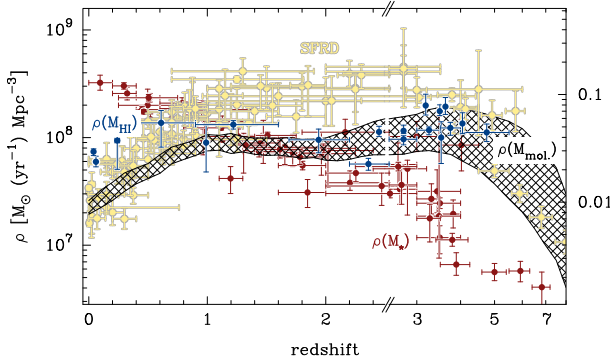
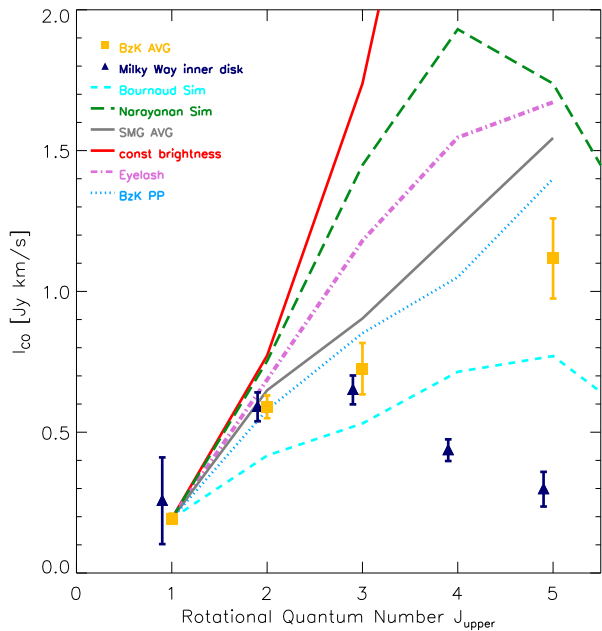


Fig. 11 Redshift-evolution of the comoving mass density (cf. *scale on left*) of molecular gas, $\rho(M_{\text{mol.}}$). The *hatched region* shows the evolution inferred from the integration of the predicted molecular gas MFs in Fig. 10 (extended to $z > 2.5$ with a set of assumptions that successfully match high- z stellar MFs and UV-LFs, e.g. González et al. 2010; Bouwens et al. 2011). The evolution of $\rho(M_{\text{mol.}})$ is compared to compilations of the cosmic evolution of the atomic hydrogen abundance ($\rho(M_{\text{HI}})$; e.g. Bauermeister et al. 2010, *blue symbols*) and of $\rho(M_{\star})$, the stellar mass density (*red symbols*; see, e.g., compilation in Marchesini et al. 2008). *Yellow symbols*—SFRD-evolution (cf. *scale on right*), as constrained by literature data

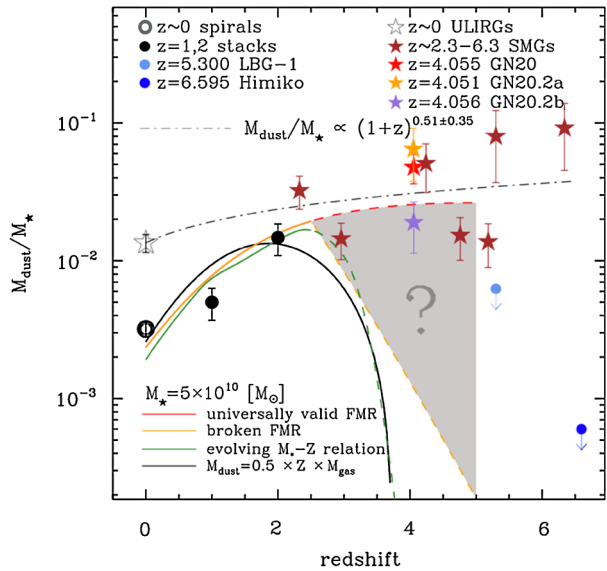
Fig. 12 Comparison of the average SLED of BzK galaxies to the MW SLED, the average of SMGs and the average (U)LIRGs SLED. All SLEDs are normalized to the CO[1-0] of the average BzK galaxy SLED, except the MW which is normalized using CO[2-1]. The results models and simulations are also shown. See Daddi et al. (2015) for references. We notice that the average SLED of lensed SPT sources (Spilker et al. 2014) is similar to that of SMGs



2.2.5 Going to Earlier Epochs

Star formation in the high- z Universe beyond $z \sim 3$ has been so far very well studied in the UV, but detailed IR investigations (required to trace dusty star formation and study the gas content) have become potentially feasible only since the advent of ALMA, as they require exquisite sensitivity. Initial results are coming in, and many more will come in the near future. In the meanwhile, a general worry to keep in mind, which could adversely af-

Fig. 13 The redshift evolution of dust to stellar mass ratios, for Main Sequence (*circles*) and Starburst (*stars*) galaxies, see Tan et al. (2014) for details and references. The (uncertain) evolution in the metallicity of massive galaxies at high redshift could imply a rapid drop of dust masses at $z > 4$



fect IR observations in the distant Universe is the possible general decline of metallicities, suggested to increase its pace earlier than $z \sim 3$ (e.g., Troncoso et al. 2014; Onodera et al., 2016). In turn, lowering the metallicity (Z) also dust masses are decreased, as one can write approximately $M_{dust} \sim 0.5 \times Z \times M_{gas}$ (roughly half of the metals being caught in dust). The possible evolution of dust to stellar mass ratios is depicted in Fig. 13. This could make IR fluxes of galaxies substantially fainter, especially in the Rayleigh-Jeans tail which is more directly proportional to the dust mass present, while the overall IR luminosity might be kept high by an increase of dust temperature. Early confirmation of these effects to $z \sim 4$ were provided by Béthermin et al. (2015). In turn, CO emission could be adversely affected as well as a roughly constant M_{dust}/LCO ratio is expected and observed at $z < 3$ for normal galaxies (Tan et al. 2013). Observations of distant GRBs could help shedding light on this issue (e.g., see Laskar et al. 2011).

2.3 Summary of Section 2

Motivated by the homogeneity of the bulk of SFGs (in particular those occupying the so-called “main sequence” of SFGs) across a broad range of redshift we have presented a simple framework (2-SFM) for the prediction of basic properties of the star-forming population. By explicitly distinguishing between (1) the population of ‘normal’ galaxies residing on the star-forming main sequence, and (2) starbursting galaxies for which we assume different characteristics (e.g. IR SEDs or a burst-dependent continuum of SFE enhancements) based our currently best observational understanding, we show that this simple description is capable of reproducing the evolution of the IR LF out to $z \sim 2.5$ and IR/radio source counts at 24 to 1100 μm and 1.4 GHz, and the distribution of IR light among dark matter halos. We use the 2-SFM framework to predict the molecular gas mass function (and CO(1 \rightarrow 0) luminosity function of SFGs, a fundamental observable which so far has only been measured at $z = 0$ and the extension of which to higher redshift is a major goal of the ALMA era. The strong evolution of the inferred H_2 -mass function to higher masses with increasing redshift suggest that the cosmic H_2 -abundance was ~ 5 times larger at the peak

of the cosmic SFH than in the local universe. Furthermore, we provide strong evidence that the higher gas fractions in distant galaxies are directly reflected in the higher sSFR of these systems. We discuss evidences for the evolution of ISM properties of galaxies to $z = 2-4$, manifested in higher dust temperatures and higher CO excitations. Further investigations at higher redshifts will be soon possible thanks to ALMA, barring the possible adverse effect of declining metallicities at high redshifts.

3 Galaxy Formation at High Redshift using Cosmological Hydrodynamic Simulations

Over the past quarter of a century, computational astrophysicists have been making tremendous advances in simulating structure formation in the Universe from shortly after the last scattering surface to the present time. In this section, we summarize some of the recent highlights of the study of high- z galaxy formation using cosmological hydrodynamic simulations.

Astronomers now have a standard cosmological model, the Λ cold dark matter (CDM) model, which can be described well with only six cosmological parameters: $(\Omega_M, \Omega_\Lambda, \Omega_b, h, \sigma_8, n_s) \approx (0.3, 0.7, 0.04, 0.7, 0.8, 0.96)$ (Komatsu et al. 2011; Hinshaw et al. 2013; Planck Collaboration et al. 2015). This simple fact itself is a remarkable achievement, and it is one of the highlights of cosmological studies obtained from the temperature anisotropy of cosmic microwave background (CMB) radiation. The predicted power spectrum of matter density fluctuations agrees well with various observational estimates, including CMB, galaxy clustering, number density of galaxy clusters, weak lensing, and Lyman- α forest (Tegmark et al. 2004). The collisionless dark matter (DM) in the Λ CDM model provides the back-bone of structure in our Universe, and it describes the matter density distribution very well on scales greater than ~ 1 Mpc. For example, nowadays one can easily run a simple N-body simulation with $\sim 500^3$ particles, which can reproduce the network of filamentary structures harboring dark matter halos and galaxies. The big question is, “Can we understand galaxy formation in the cosmological context of Λ CDM model?”

Based on the Λ CDM model, we now understand the cosmic time-line relatively well. Starting from the Big Bang at 13.8 billion years ago, the cosmic gas in our Universe experienced a major transition from being optically thick to thin, when the electrons combined with protons, and the Universe became transparent to the photons at $z \sim 1100$ (i.e., ‘reionization’ of the Universe). We now observe these photons as the CMB radiation that have traveled from the ‘last scattering surface’ to the present time without being scattered randomly.

From $z \sim 1100$ to $z \sim 20$, the ‘dark ages’ continued, during which the intergalactic medium (IGM) was fully neutral and there were no light sources in the Universe. Then the ‘first stars’ started to form in DM halos with masses $M_h \sim 10^6 M_\odot$, and the bubbles of ionized region (i.e., the Stromgren spheres) expanded and percolated gradually (e.g., Iliev et al. 2006). Shortly after, the ‘first galaxies’ started to form in DM halos in the atomic-cooling halos with virial temperatures greater than $T \sim 10^4$ K and $M_h \sim 10^8 M_\odot$. It is widely believed that these first stars and first galaxies are the sources which provided the ionizing photons necessary to reionize the Universe (e.g., Iliev et al. 2006; Yajima et al. 2011). From the measurements of electron scattering optical depth by CMB, it is estimated that the reionization took place at around $z \sim 6-11$ (Hinshaw et al. 2013; Planck Collaboration et al. 2015), and the Gunn-Peterson trough in the quasar spectrum tells us that the reionization was completed by $z \sim 6$ (Fan et al. 2006).

The first stars and first galaxies also enriched the IGM for the first time, and the metals change the cooling rate of gas in later galaxy formation processes via metal-line cooling. Therefore understanding the formation of first galaxies and evaluating their number density is important for both cosmology and galaxy formation theory. One of the key physical parameters that we need to determine is the escape fraction of ionizing photons, f_{esc} , from first galaxies as we will discuss further in the following subsections.

Galaxies have complex internal structures, e.g., bulge, disk, halo. The disk exhibits spiral arms, and the bulge size varies from galaxies to galaxies. In order to estimate f_{esc} , we need to understand the structures of galaxies better, and how the stars and gas are distributed within in them. This means that we want to understand the disappearance of the Hubble Sequence towards high-redshift, and how the SFR changes over time in different galaxies. One method to characterize the star formation in galaxies is to examine the Kennicutt-Schmidt relation, which has been performed extensively at low redshift as described in earlier sections. The same can be done at higher redshifts with ALMA, and computer simulations can provide useful information on galactic structure evolution at high-redshift where observational data are still scarce.

3.1 Computational Cosmology

To understand the history of structure formation in the Universe, computational cosmology (or numerical cosmology) provides a useful method, where we try to follow the formation and evolution of structures in our Universe self-consistently from first principles as much as possible. We start from the initial condition that is consistent with the fluctuations observed in the temperature fluctuations of CMB, then prepare a universe in a supercomputer assuming a set of cosmological parameters; namely, dark energy, dark matter, and baryons in an expanding universe. And then we simulate the structure formation as a function of time using the laws of gravity and fluid dynamics. The hope is to reproduce the Universe as we observe today at $z = 0$, after the simulation is evolved from $z \sim 200$ to $z = 0$.

To form galaxies in cosmological simulations, one has to include additional physics, such as radiative cooling and heating, star formation (SF), and feedback. For example, we use the modified version of GADGET-3 smoothed particle hydrodynamics (SPH) code (Springel 2005), which includes radiative heating by UV background radiation, cooling by H, He and metals (Choi and Nagamine 2009), multi-component variable velocity (MVV) wind model for supernova (SN) feedback (Choi and Nagamine 2011), self-shielding effect of UV background (Nagamine et al. 2010). The treatment of self-shielding is important for these cosmological simulations, and follow-up work have shown that our treatment works well to simulate HI absorbers (Bird et al. 2013).

The resolution of these cosmological simulations depend on the box size and particle counts. For example, our simulations have box sizes of $10\text{--}100 h^{-1} \text{Mpc}$, the particle count ranges from 2×144^3 to 2×600^3 , comoving gravitational softening length of a comoving few kpc to $700 h^{-1} \text{pc}$. A simulation with 2×600^3 particles in a comoving $10 h^{-1} \text{Mpc}$ has a dark matter particle mass of $2.78 \times 10^5 h^{-1} M_{\odot}$, gas particle mass of $5.65 \times 10^4 h^{-1} M_{\odot}$, and gravitational softening length of comoving $670 h^{-1} \text{pc}$. Usually it is difficult to cover a wide range of dark matter halo masses in one simulation box, therefore, we use different comoving box sizes (e.g., 10, 34, $100 h^{-1} \text{Mpc}$) to cover a wide range of $M_h = 10^8\text{--}10^{13} h^{-1} M_{\odot}$. This composite method allows us to also examine galaxies with stellar masses $M_{\star} = 10^7\text{--}10^{11} h^{-1} M_{\odot}$ (Jaacks et al. 2012), from dwarfs to moderately massive galaxies.

In our simulations, the star formation is treated either by the fiducial pressure-based SF model (Schaye and Dalla Vecchia 2008; Choi and Nagamine 2010) or the H_2 -based

SF model (Thompson et al. 2014). With the mass and spatial resolution given above for cosmological hydrodynamic simulations, it is still not possible to resolve the formation and destruction of giant molecular clouds in detail. Therefore many research groups resort to various subgrid multiphase interstellar medium (ISM) models, where each SPH particle is pictured as a multiphase hybrid gas (Yepes et al. 1997; Springel and Hernquist 2003). Only the thermodynamics of the hot phase is followed here, while the cold phase is assumed to stay cold with $T \sim 10^4$ K. The exchange of energy and mass between the hot and cold phase is assumed to be in equilibrium, as the exchanges in high-density regions take place on a much shorter time-scale than the global simulation time-steps.

The star formation is typically computed with an equation similar to $\dot{\rho}_* = (1 - \beta)\rho_c/t_*$, where β is the instantaneous recycling fraction of gas after supernova explosions, and ρ_c is the cold phase gas density. The SF time-scale, t_* , is usually taken to be proportional to the dynamical time of the gas, i.e., $t_* = t_*^0(\rho_g/\rho_{\text{th}})^{-0.5}$, where the normalization $t_*^0 \sim 2$ Gyr is needed to reproduce the observed normalization of Kennicutt-Schmidt law, and ρ_{th} is the SF threshold density. One of the problems of such simple SF law is that it does not have an explicit dependence on metallicity. Therefore we have revised our model and adopted the H₂-based SF law (Thompson et al. 2014), where the H₂ mass fraction is computed for each SPH particle and the H₂ mass density is used for the SF law instead of total cold gas density. Since the H₂ fraction is dependent on the gas metallicity Krumholz et al. (2009), this introduces the metallicity dependence of SFR naturally through the abundance of H₂ molecules. The H₂ molecules form on dust, and the model of Krumholz et al. (2009) provided simple approximate formulae to estimate H₂ fraction as a function of gas surface density and metallicity.

The effect of supernova feedback is considered, and a part of SN energy is given to nearby SPH particles as a kinetic energy. There are various ways of distributing SN energy, but some form of efficient kinetic feedback is necessary to distribute the metals and energy into the IGM. In the case of the MVV wind model by (Choi and Nagamine 2011), we compute the galactic properties such as stellar mass and SFR by grouping the star/gas/DM particles on the fly as the simulation runs, and compute the wind velocity based on the SFR of individual galaxies. Such a scaling between galactic wind velocity and galaxy SFR (or stellar mass) has been suggested by some observations of high-*z* galaxies (Weiner et al. 2009).

Once the star particles are created based on the above SFR estimate, each star particle carries physical tags such as the stellar mass, formation time, and metallicity. Based on these quantities, we can apply population synthesis models (e.g., Bruzual and Charlot 2003) to each star particle and compute the spectral output of simulated galaxies. Of course the simulation examples that we describe in this section is a limited example, and there have been other extensive efforts by many groups. For example, the Illustris project (e.g., Genel et al. 2014; Vogelsberger et al. 2014) and EAGLE simulations (Schaye et al. 2015) have performed even larger cosmological hydrodynamic simulations than described in this article and provided large galaxy catalogues to the astronomical community.

3.2 Evolution of Galaxy Stellar and Luminosity Functions at High-*z*

One of the key statistics for galaxy formation and evolution is the galaxy stellar mass function (GSMF) and luminosity function (LF). The shapes of these functions at $z = 0$ have been constrained well (Blanton et al. 2001; Cole et al. 2001), and they can be fit well with the Schechter function. However, the situation at higher redshift is more uncertain, in particular the faint-end slope, α , is not constrained well yet. At $z = 0$, the slope is $\alpha \sim -1.2$, and it becomes steeper to $\alpha \sim -1.6$ at $z \sim 3$ (Reddy and Steidel 2009).

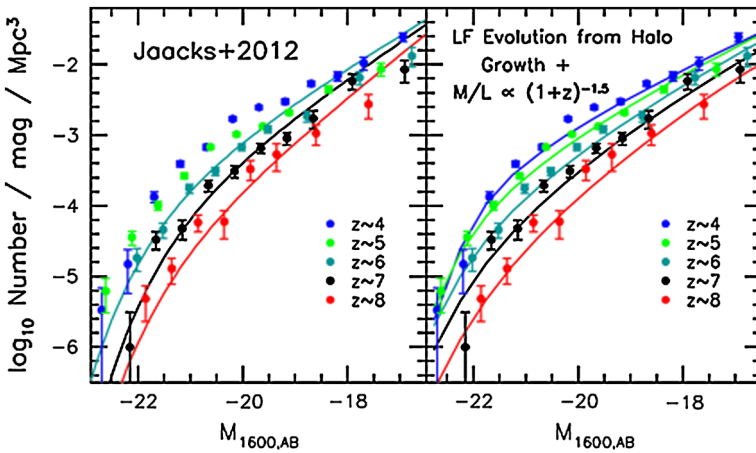


Fig. 14 Comparison of galaxy luminosity functions at $z = 4\text{--}8$ between cosmological hydrodynamic simulation (Jaacks et al. 2012, left panel) and observations (Fig. 19 of Bouwens et al. 2015). In both panels, the observational data is shown as data points, and either simulation or a simple model results are shown with Schechter fits. Both panels show the steepening of the faint-end slope α with increasing redshift at $z > 4$, e.g., from $\alpha = -1.64$ ($z = 4$) to -2.06 ($z = 6$)

Using the results of cosmological hydrodynamic simulations, several groups have shown that the GSMF and LF become steeper at the faint-end with increasing redshift, from $\alpha = -1.6$ at $z \sim 3$ to even $\alpha \sim -2$ at $z \sim 6$ (e.g., Nagamine et al. 2004; Night et al. 2006; Finlator et al. 2006; Lo Faro et al. 2009). More recent work has extended the comparison to $z > 6$, and some simulations indicated that the slope could become even steeper with $\alpha < -2.0$ (Jaacks et al. 2012; Bouwens et al. 2015), as shown in Fig. 14. However, the initial work by Jaacks et al. (2012) used an SF model which does not have any dependence on metallicity, and this may have led to a slight overestimation of SF efficiency at high- z .

Jaacks et al. (2013) have examined the impact of lower metallicity on GSMF at high- z using the H_2 -based SF model of Thompson et al. (2014). In this SF model, the mass fraction of molecular hydrogen, f_{H_2} , is computed within the framework of multiphase ISM model of Springel and Hernquist (2003), and f_{H_2} becomes lower with decreasing metallicity because H_2 molecules form on dust. Figure 15 shows the star formation rate (SFR) function at $z = 6\text{--}8$, in comparison with the observational data by Smit et al. (2012). The SFR function provides a more direct comparison between simulations and observations, as SFR is a more direct output from the simulation rather than spectral output that has to be computed by a population synthesis code with an assumption of a stellar initial mass function (IMF). The simulation with the H_2 -based SF model yielded a flatter faint-end slope at $\text{SFR} < 1 M_{\odot} \text{yr}^{-1}$, which corresponds to a limiting rest-frame UV magnitude of $M_{\text{UV}} \sim -16$. Within the observed range of magnitudes, the simulation result agrees very well with the observed data (red crosses). The flatter faint-end slope and the break at $\text{SFR} \sim 1 M_{\odot} \text{yr}^{-1}$ is caused by the inefficient star formation at low metallicities in faint galaxies at high- z in our simulations.

The faint-end slope of GSMF and LF is quite important for the ionizing photon budget, as these faint galaxies are the ones that provided the photons necessary to reionize the Universe. Jaacks et al. (2013) have shown that, even with the reduced number of faint galaxies with the H_2 -based SF model, these galaxies can provide a sufficient number of ionizing photons for reionization by $z \sim 6$, and the contribution is in fact dominated by the lower mass and fainter galaxies with $M_{\star} \leq 10^8 M_{\odot}$.

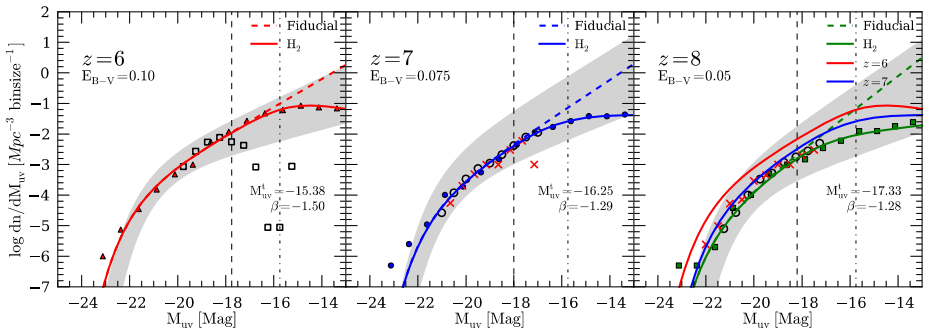


Fig. 15 SFR function at $z = 6, 7, 8$ in cosmological hydrodynamic simulations with H_2 -based SF model (adopted from Jaacks et al. 2013). The data points are mostly simulation data, and the *red crosses* are the observed data by Smit et al. (2012). The fits shown by the *solid lines* are the modified Schechter function with an additional break at the faint-end, and the fits for $z = 6, 7, 8$ are compared in the *right-most panel*, where we can see that the galaxies become brighter and more numerous from $z = 8$ to $z = 6$. The *grey shade* is the range of Schechter fits to the observed data by Bouwens et al. (2011)

Integrating the observed galaxy UV luminosity function can give the estimates of UV luminosity density, which can be converted to the cosmic SFR density with an assumption of an IMF. However, since current galaxy observations cannot probe the faintest galaxies that might exist at high-redshift at $M_{UV} > -15$, it is difficult to constrain the SFR density accurately at high- z . Using GRBs can be useful in this context, as it is very bright and could be detected as high redshift as $z > 8$ (Kistler et al. 2009; Tanvir et al. 2009). These initial estimates, albeit from a very small sample, gives higher value of cosmic SFR density at $z > 6$ than the estimates based on UV luminosity function of galaxies.

A more proper treatment of ionizing photon budget requires a radiative transfer calculation to estimate the escape fraction of ionizing photons from galaxies, and there have been a number of interesting works that gave varying results on the values of f_{esc} based on radiative transfer calculations (e.g., Gnedin et al. 2008; Wise and Cen 2009; Razoumov and Sommer-Larsen 2010; Paardekooper et al. 2011). Yajima et al. (2011, 2015) have shown that f_{esc} is a decreasing function of halo mass at high- z , although with a large dispersion particularly for lower mass galaxies (Fig. 16). Significant amounts of gas around star-forming regions prevent the escape of ionizing photons in massive galaxies, whereas the gas distribution is somewhat more irregular in low-mass galaxies, enabling the photons to escape in a preferential direction. Folding in the estimated values of f_{esc} of each galaxies into the calculation of ionizing photon budget, they estimated that the faint galaxies at $z \geq 6$ can provide sufficient number of ionizing photons thanks to their large f_{esc} .

GRBs can also help to set constraints on f_{esc} of high- z galaxies. For example, Chen et al. (2007) showed that one can estimate f_{esc} of ionizing photons using the afterglows of long GRBs based on the optical depth of neutral hydrogen column density in the host ISM, free from the background subtraction uncertainties. This method is potentially very useful, because it can provide estimates of f_{esc} of sub- L^* galaxies where most GRBs occur and otherwise difficult to observe directly. These faint galaxies at the fainter end of the luminosity functions contributed the most to the ionizing photon budget, therefore having observational estimates of f_{esc} for these low-mass galaxies is quite important for the study of reionization of the Universe. Both Chen et al. (2007) and Fynbo et al. (2009) found small mean values of $\langle f_{esc} \rangle \sim 0.02$, however larger values have also been suggested by observations (e.g., Inoue et al. 2006; Smith et al. 2016) and from models based on GRB and galaxy observations (Wyithe et al. 2010; Dijkstra et al. 2014).

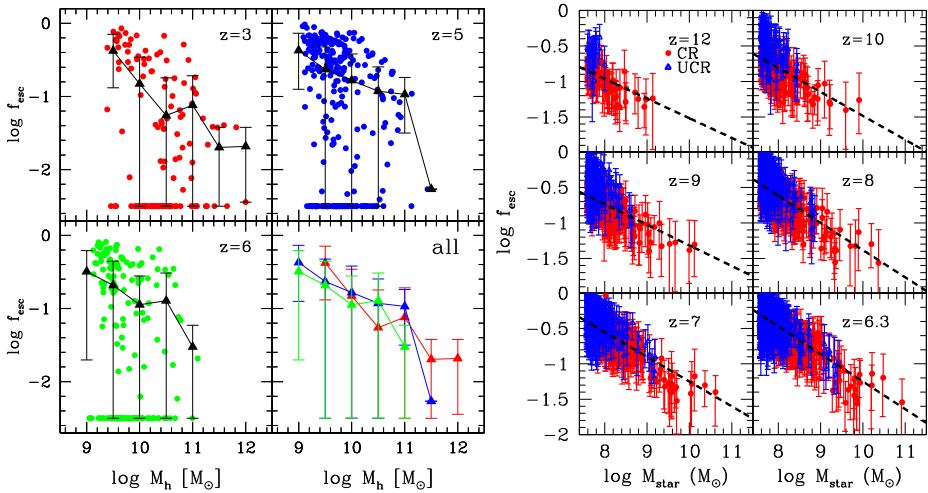
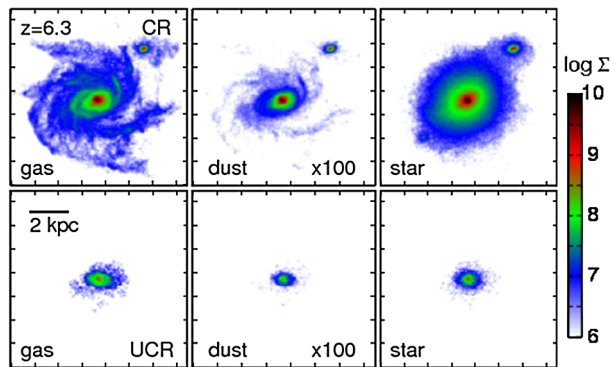


Fig. 16 Escape fraction of ionizing photons at $z = 3\text{--}6$ in cosmological SPH simulations (panel (a), Yajima et al. 2011), and that of UV photons from $z = 12$ to $z = 6$ (panel (b), Yajima et al. 2015). In general, it is a declining function with increasing M_h , but with a large scatter for lower mass galaxies in particular. Also there doesn't seem to be strong evolution in the relation from $z = 6$ to $z = 3$

Fig. 17 Massive disk galaxy at $z \sim 6$ found in a cosmological SPH simulation (Yajima et al. 2015). The *upper row* represents the most massive galaxy in the constrained realization of a high-density region ($M_{\text{star}} \sim 8.4 \times 10^{10} M_{\odot}$ and $M_{\text{gas}} \sim 4.8 \times 10^{10} M_{\odot}$). The *lower row* shows the most massive galaxy in the less dense, unconstrained region with $M_{\text{star}} \sim 1.5 \times 10^9 M_{\odot}$ and $M_{\text{gas}} \sim 3.1 \times 10^9 M_{\odot}$



Romano-Díaz et al. (2011) and Yajima et al. (2015) found the existence of massive spiral disk galaxies at high redshift ($z \sim 10$ and 6, respectively) using zoom-in cosmological hydrodynamic simulations of a high-density region, as shown in Fig. 17. These massive galaxies contain a fair amount of dust, and therefore might be good targets for ALMA observations. In fact bright quasars have been already detected by ALMA via [CII] line (e.g., Maiolino et al. 2005), and perhaps ALMA can extend these detections down to lower mass-scale objects in the near future.

As these recent works have shown, it seems now possible to form massive disk galaxies *for a certain feedback models* at high-redshift in zoom-in cosmological hydrodynamic with sub-kpc resolution. Although Yajima et al. (2015) found a nice disk geometry for a massive galaxy in a high-density region at high-redshift, some of the more recent high-resolution zoom-in simulations employ more direct momentum injection rather than relying on sub-resolution kinetic feedback model (e.g., Hopkins et al. 2013; Muratov et al. 2015), and these more direct feedback models seem to be more efficient in ejecting gas from high- z star-

forming galaxies, often disrupting the disk galaxy geometry. More future studies of galaxy formation will be performed using cosmological hydrodynamic simulations, and the impact of both supernova and AGN feedback will be assessed in more detail, giving insight into the mechanism of forming the main sequence of star formation and downsizing of galaxies.

Acknowledgements The authors would like to thank the organizers of the workshop “Gamma-Ray Bursts: A Tool to Explore the Young Universe”, and in particular Emeric Le Floc’h, for inviting us to discuss the subject in this chapter. K. Nagamine acknowledges the partial support by JSPS KAKENHI Grant Number 26247022, the HST grant AR-12143.01-A provided by NASA through a grant from the Space Telescope Science Institute, which is operated by the Association of Universities for Research in Astronomy, Incorporated, under NASA contract NAS5-26555.

References

- A.R. Basu-Zych, B.D. Lehmer, A.E. Hornschemeier, T.S. Gonçalves, T. Fragos, T.M. Heckman, R.A. Overzier, A.F. Ptak, D. Schiminovich, *Astrophys. J.* **774**, 152 (2013)
- A. Bauermeister, L. Blitz, C.-P. Ma, *Astrophys. J.* **717**, 323 (2010)
- P.S. Behroozi, R.H. Wechsler, C. Conroy, *Astrophys. J.* **770**, 57 (2013)
- E.F. Bell et al., *Astrophys. J.* **663**, 834 (2007)
- E. Berger, B.E. Penprase, S.B. Cenko, S.R. Kulkarni, D.B. Fox, C.C. Steidel, N.A. Reddy, Spectroscopy of GRB 050505 at $z = 4.275$: a $\log N(\text{HI}) = 22.1$ DLA host galaxy and the nature of the progenitor. *Astrophys. J.* **642**, 979–988 (2006). doi:[10.1086/501162](https://doi.org/10.1086/501162)
- M. Béthermin, H. Dole, G. Lagache, D. Le Borgne, A. Penin, *Astron. Astrophys.* **529**, A4 (2011)
- M. Béthermin, E. Daddi, G. Magdis et al., *Astrophys. J. Lett.* **757**, L23 (2012b)
- M. Béthermin et al., *Astron. Astrophys.* **557**, A66 (2013)
- M. Béthermin et al., *Astron. Astrophys.* **567**, 103 (2014)
- M. Béthermin et al., *Astron. Astrophys.* **573**, 113 (2015)
- S. Bird, M. Vogelsberger, D. Sijacki, M. Zaldarriaga, V. Springel, L. Hernquist, Moving-mesh cosmology: properties of neutral hydrogen in absorption. *Mon. Not. R. Astron. Soc.* **429**, 3341–3352 (2013). doi:[10.1093/mnras/sts590](https://doi.org/10.1093/mnras/sts590)
- M.R. Blanton, J. Dalcanton, D. Eisenstein, J. Loveday, M.A. Strauss, M. SubbaRao, D.H. Weinberg, J.E.J. Anderson, et al., The luminosity function of galaxies in sdss commissioning data. *Astron. J.* **121**, 2358 (2001)
- M. Boquien, V. Buat, A. Boselli, M. Baes, G.J. Bendo, L. Ciesla, A. Cooray, L. Cortese, S. Eales, G. Gavazzi, H.L. Gomez, V. Leboutteiller, C. Pappalardo, M. Pohlen, M.W.L. Smith, L. Spinoglio, *Astron. Astrophys.* **539**, A145 (2012)
- F. Bournaud, E. Daddi, A. Weiß, F. Renaud, C. Mastropietro, R. Teyssier, *Astron. Astrophys.* **575**, A56 (2015)
- R.J. Bouwens, G.D. Illingworth, P.A. Oesch, I. Labbé, M. Trenti, P. van Dokkum, M. Franx, M. Stiavelli, C.M. Carollo, D. Magee, V. Gonzalez, Ultraviolet luminosity functions from 132 $z \sim 7$ and $z \sim 8$ Lyman-break galaxies in the ultra-deep HUDF09 and wide-area early release science WFC3/IR observations. *Astrophys. J.* **737**, 90 (2011). doi:[10.1088/0004-637X/737/2/90](https://doi.org/10.1088/0004-637X/737/2/90)
- R.J. Bouwens, G.D. Illingworth, P.A. Oesch, M. Trenti, I. Labbé, L. Bradley, M. Carollo, P.G. van Dokkum, V. Gonzalez, B. Holwerda, M. Franx, L. Spitler, R. Smit, D. Magee, UV luminosity functions at redshifts $z \sim 4$ to $z \sim 10$: 10000 galaxies from HST legacy fields. *Astrophys. J.* **803**, 34 (2015). doi:[10.1088/0004-637X/803/1/34](https://doi.org/10.1088/0004-637X/803/1/34)
- J. Brinchmann, S. Charlot, S.D.M. White et al., *Mon. Not. R. Astron. Soc.* **351**, 1151 (2004)
- G. Bruzual, S. Charlot, Stellar population synthesis at the resolution of 2003. *Mon. Not. R. Astron. Soc.* **344**, 1000 (2003)
- V. Buat, S. Noll, D. Burgarella, E. Giovannoli, V. Charmandaris, M. Pannella, H.S. Hwang, D. Elbaz, M. Dickinson, G. Magdis, N. Reddy, E.J. Murphy, *Astron. Astrophys.* **545**, A141 (2012)
- D. Calzetti, L. Armus, R.C. Bohlin, A.L. Kinney, J. Koornneef, T. Storchi-Bergmann, The dust content and opacity of actively star-forming galaxies. *Astrophys. J.* **533**, 682 (2000)
- C.M. Casey, D. Narayanan, A. Cooray, *Phys. Rep.* **541**, 45 (2014)
- H.-W. Chen, J.X. Prochaska, N.Y. Gnedin, A new constraint on the escape fraction in distant galaxies using γ -ray burst afterglow spectroscopy. *Astrophys. J. Lett.* **667**, 125–128 (2007). doi:[10.1086/522306](https://doi.org/10.1086/522306)
- J.-H. Choi, K. Nagamine, Effects of metal enrichment and metal cooling in galaxy growth and cosmic star formation history. *Mon. Not. R. Astron. Soc.* **393**, 1595–1607 (2009). doi:[10.1111/j.1365-2966.2008.14297.x](https://doi.org/10.1111/j.1365-2966.2008.14297.x)

- J.-H. Choi, K. Nagamine, Effects of cosmological parameters and star formation models on the cosmic star formation history in Λ CDM cosmological simulations. *Mon. Not. R. Astron. Soc.* **407**, 1464–1476 (2010). doi:[10.1111/j.1365-2966.2010.17029.x](https://doi.org/10.1111/j.1365-2966.2010.17029.x)
- J.-H. Choi, K. Nagamine, Multicomponent and variable velocity galactic outflow in cosmological hydrodynamic simulations. *Mon. Not. R. Astron. Soc.* **410**, 2579–2592 (2011). doi:[10.1111/j.1365-2966.2010.17632.x](https://doi.org/10.1111/j.1365-2966.2010.17632.x)
- S. Cole, P. Norberg, C.M. Baugh, C.S. Frenk, J. Bland-Hawthorn, T. Bridges, R. Cannon, M. Colless, C. Collins, W. Couch, N. Cross, G. Dalton, R. De Propris, S.P. Driver, G. Efstathiou, R.S. Ellis, K. Glazebrook, C. Jackson, O. Lahav, I. Lewis, S. Lumsden, S. Maddox, D. Madgwick, J.A. Peacock, B.A. Peterson, W. Sutherland, K. Taylor, The 2dF galaxy redshift survey: near-infrared galaxy luminosity functions. *Mon. Not. R. Astron. Soc.* **326**, 255–273 (2001). doi:[10.1046/j.1365-8711.2001.04591.x](https://doi.org/10.1046/j.1365-8711.2001.04591.x)
- A. Cucchiara, M. Fumagalli, M. Rafelski, D. Kocevski, J.X. Prochaska, R.J. Cooke, G.D. Becker, *Astrophys. J.* **804**, 51 (2015)
- E. Daddi, M. Dickinson, G. Morrison, R. Chary, A. Cimatti, D. Elbaz, D. Frayer, A. Renzini, A. Pope, D.M. Alexander, F.E. Bauer, M. Giavalisco, M. Huynh, J. Kurk, M. Mignoli, *Astrophys. J.* **670**, 156 (2007)
- E. Daddi et al., *Astrophys. J.* **713**, 686 (2010a)
- E. Daddi et al., *Astrophys. J. Lett.* **714**, L118 (2010b)
- E. Daddi et al., *Astron. Astrophys.* **577**, A46 (2015)
- D.A. Dale, S.A. Cohen, L.C. Johnson, M.D. Schuster, D. Calzetti, C.W. Engelbracht, A. Gil de Paz, R.C. Kennicutt, J.C. Lee, A. Begum, M. Block, J.J. Dalcanton, J.G. Funes, K.D. Gordon, B.D. Johnson, A.R. Marble, S. Sakai, E.D. Skillman, L. van Zee, F. Walter, D.R. Weisz, B. Williams, S.-Y. Wu, Y. Wu, *Astrophys. J.* **703**, 517 (2009)
- H. Dannerbauer, E. Daddi, D.A. Riechers et al., *Astrophys. J. Lett.* **698**, L178 (2009)
- R. Davé, *Mon. Not. R. Astron. Soc.* **385**, 147 (2008)
- P. Di Matteo, F. Combes, A.-L. Melchior, B. Semelin, *Astron. Astrophys.* **468**, 61 (2007)
- M. Dijkstra, S. Wyithe, Z. Haiman, A. Mesinger, L. Pentericci, Evolution in the escape fraction of ionizing photons and the decline in strong Ly α emission from $z > 6$ galaxies. *Mon. Not. R. Astron. Soc.* **440**, 3309–3316 (2014). doi:[10.1093/mnras/stu531](https://doi.org/10.1093/mnras/stu531)
- A. Domínguez, B. Siana, A.L. Henry, C. Scarlata, A.G. Bedregal, M. Malkan, H. Atek, N.R. Ross, J.W. Colbert, H.I. Teplitz, M. Rafelski, P. McCarthy, A. Bunker, N.P. Hathi, A. Dressler, C.L. Martin, D. Masters, *Astrophys. J.* **763**, 145 (2013)
- D. Elbaz, M. Dickinson, H.S. Hwang et al., *Astron. Astrophys.* **533**, A119 (2011)
- D.K. Erb, A.E. Shapley, M. Pettini, C.C. Steidel, N.A. Reddy, K.L. Adelberger, *Astrophys. J.* **644**, 813 (2006a)
- D.K. Erb, C.C. Steidel, A.E. Shapley, M. Pettini, N.A. Reddy, K.L. Adelberger, *Astrophys. J.* **646**, 107 (2006b)
- X. Fan, C.L. Carilli, B. Keating, Observational constraints on cosmic reionization. *Annu. Rev. Astron. Astrophys.* **44**, 415–462 (2006). doi:[10.1146/annurev.astro.44.051905.092514](https://doi.org/10.1146/annurev.astro.44.051905.092514)
- R. Feldmann, N.Y. Gnedin, A.V. Kravtsov, *Astrophys. J.* **747**, 124 (2012)
- K. Finlator, R. Davé, *Mon. Not. R. Astron. Soc.* **385**, 2181 (2008)
- K. Finlator, R. Davé, C. Papovich, L. Hernquist, The physical and photometric properties of high-redshift galaxies in cosmological hydrodynamic simulations. *Astrophys. J.* **639**, 672–694 (2006). doi:[10.1086/499349](https://doi.org/10.1086/499349)
- M. Fioc, B. Rocca-Volmerange, *Astron. Astrophys.* **326**, 950 (1997)
- J.P.U. Fynbo, P. Jakobsson, J.X. Prochaska, D. Malesani, C. Ledoux, A. de Ugarte Postigo, M. Nardini, P.M. Vreeswijk, K. Wiersema, J. Hjorth, J. Sollerman, H.-W. Chen, C.C. Thöne, G. Björnsson, J.S. Bloom, A.J. Castro-Tirado, L. Christensen, A. De Cia, A.S. Fruchter, J. Gorosabel, J.F. Graham, A.O. Jaunsen, B.L. Jensen, D.A. Kann, C. Kouveliotou, A.J. Levan, J. Maund, N. Masetti, B. Milvang-Jensen, E. Palazzi, D.A. Perley, E. Pian, E. Rol, P. Schady, R.L.C. Starling, N.R. Tanvir, D.J. Watson, D. Xu, T. Augsteijn, F. Grundahl, J. Telting, P.-O. Quirion, Low-resolution spectroscopy of gamma-ray burst optical afterglows: biases in the swift sample and characterization of the absorbers. *Astrophys. J. Suppl. Ser.* **185**, 526–573 (2009). doi:[10.1088/0067-0049/185/2/526](https://doi.org/10.1088/0067-0049/185/2/526)
- J.E. Geach, I. Smail, S.M. Moran, L.A. MacArthur, C.d.P. Lagos, A.C. Edge, *Astrophys. J. Lett.* **730**, L19 (2011)
- S. Genel, M. Vogelsberger, V. Springel, D. Sijacki, D. Nelson, G. Snyder, V. Rodriguez-Gomez, P. Torrey, L. Hernquist, Introducing the illustris project: the evolution of galaxy populations across cosmic time. *Mon. Not. R. Astron. Soc.* **445**, 175–200 (2014). doi:[10.1093/mnras/stu1654](https://doi.org/10.1093/mnras/stu1654)
- R. Genzel et al., *Mon. Not. R. Astron. Soc.* **407**, 2091 (2010)
- R. Genzel, L.J. Tacconi, F. Combes et al., *Astrophys. J.* **746**, 69 (2012)
- R. Genzel et al., *Astrophys. J.* **800**, 20 (2015)

- N.Y. Gnedin, A.V. Kravtsov, H. Chen, Escape of ionizing radiation from high-redshift galaxies. *Astrophys. J.* **672**, 765–775 (2008). doi:[10.1086/524007](https://doi.org/10.1086/524007)
- V. González, I. Labbé, R.J. Bouwens et al., *Astrophys. J.* **713**, 115 (2010)
- J. Graciá-Carpio, E. Sturm, S. Hailey-Dunsheath et al., *Astrophys. J. Lett.* **728**, 7 (2011)
- B. Groves, J. Brinchmann, C.J. Walcher, *Mon. Not. R. Astron. Soc.* **419**, 1402 (2012)
- C. Gruppioni, F. Pozzi, G. Zamorani, C. Vignali, *Mon. Not. R. Astron. Soc.* **416**, 70 (2011)
- G. Hinshaw, D. Larson, E. Komatsu, D.N. Spergel, C.L. Bennett, J. Dunkley, M.R. Nolta, M. Halpern, R.S. Hill, N. Odegard, L. Page, K.M. Smith, J.L. Weiland, B. Gold, N. Jarosik, A. Kogut, M. Limon, S.S. Meyer, G.S. Tucker, E. Wollack, E.L. Wright, Nine-year Wilkinson Microwave Anisotropy Probe (WMAP) observations: cosmological parameter results. *Astrophys. J. Suppl. Ser.* **208**, 19 (2013). doi:[10.1088/0067-0049/208/2/19](https://doi.org/10.1088/0067-0049/208/2/19)
- P.F. Hopkins, T.J. Cox, L. Hernquist, D. Narayanan, C.C. Hayward, N. Murray, Star formation in galaxy mergers with realistic models of stellar feedback and the interstellar medium. *Mon. Not. R. Astron. Soc.* **430**, 1901–1927 (2013). doi:[10.1093/mnras/stt017](https://doi.org/10.1093/mnras/stt017)
- O. Ilbert, M. Salvato, E. Le Flocc'h et al., *Astrophys. J.* **709**, 644 (2010)
- I.T. Iliev, B. Ciardi, M.A. Alvarez, A. Maselli, A. Ferrara, N.Y. Gnedin, G. Mellema, T. Nakamoto, M.L. Norman, A.O. Razoumov, E.-J. Rijikhorst, J. Ritzerveld, P.R. Shapiro, H. Susa, M. Umemura, D.J. Whalen, Cosmological radiative transfer codes comparison project. I. The static density field tests. *Mon. Not. R. Astron. Soc.* **371**, 1057–1086 (2006). doi:[10.1111/j.1365-2966.2006.10775.x](https://doi.org/10.1111/j.1365-2966.2006.10775.x)
- A.K. Inoue, I. Iwata, J.-M. Deharveng, The escape fraction of ionizing photons from galaxies at $z = 0-6$. *Mon. Not. R. Astron. Soc.* **371**, 1–5 (2006). doi:[10.1111/j.1745-3933.2006.00195.x](https://doi.org/10.1111/j.1745-3933.2006.00195.x)
- J. Jaacks, J.-H. Choi, K. Nagamine, R. Thompson, S. Varghese, Steep faint-end slopes of galaxy mass and luminosity functions at $z \geq 6$ and the implications for reionization. *Mon. Not. R. Astron. Soc.* **420**, 1606–1620 (2012). doi:[10.1111/j.1365-2966.2011.20150.x](https://doi.org/10.1111/j.1365-2966.2011.20150.x)
- J. Jaacks, R. Thompson, K. Nagamine, Impact of H_2 -based star formation model on the $z \geq 6$ luminosity function and the ionizing photon budget for reionization. *Astrophys. J.* **766**, 94 (2013). doi:[10.1088/0004-637X/766/2/94](https://doi.org/10.1088/0004-637X/766/2/94)
- B.D. Johnson, D. Schiminovich, M. Seibert, M. Treyer, D.C. Martin, T.A. Barlow, K. Forster, P.G. Friedman, P. Morrissey, S.G. Neff, T. Small, T.K. Wyder, L. Bianchi, J. Donas, T.M. Heckman, Y.-W. Lee, B.F. Madore, B. Milliard, R.M. Rich, A.S. Szalay, B.Y. Welsh, S.K. Yi, *Astrophys. J. Suppl. Ser.* **173**, 392 (2007)
- A. Karim et al., *Astrophys. J.* **730**, 61 (2011)
- R.C. Kennicutt, *Annu. Rev. Astron. Astrophys.* **36**, 189 (1998)
- D. Keres, M.S. Yun, J.S. Young, *Astrophys. J.* **582**, 659 (2003)
- L.J. Kewley, S.L. Ellison, *Astrophys. J.* **681**, 1183 (2008)
- M.D. Kistler, H. Yüksel, J.F. Beacom, A.M. Hopkins, J.S.B. Wyithe, The star formation rate in the reionization era as indicated by gamma-ray bursts. *Astrophys. J. Lett.* **705**, 104–108 (2009). doi:[10.1088/0004-637X/705/2/L104](https://doi.org/10.1088/0004-637X/705/2/L104)
- E. Komatsu, K.M. Smith, J. Dunkley, C.L. Bennett, B. Gold, G. Hinshaw, N. Jarosik, D. Larson, et al., Seven-year Wilkinson Microwave Anisotropy Probe (WMAP) observations: cosmological interpretation. *Astrophys. J. Suppl. Ser.* **192**, 18 (2011). doi:[10.1088/0067-0049/192/2/18](https://doi.org/10.1088/0067-0049/192/2/18)
- X. Kong, S. Charlot, J. Brinchmann, S.M. Fall, *Mon. Not. R. Astron. Soc.* **349**, 769 (2004)
- M. Kriek, I. Labbé, C. Conroy, K.E. Whitaker et al., *Astrophys. J. Lett.* **722**, L64 (2010)
- M.R. Krumholz, C.F. McKee, J. Tumlinson, The star formation law in atomic and molecular gas. *Astrophys. J.* **699**, 850–856 (2009). doi:[10.1088/0004-637X/699/1/850](https://doi.org/10.1088/0004-637X/699/1/850)
- C.G. Lacey, C.M. Baugh, C.S. Frenk et al., *Mon. Not. R. Astron. Soc.* **405**, 2 (2010)
- T. Laskar, E. Berger, R.-R. Chary, *Astrophys. J.* **739**, 1 (2011)
- E. Le Flocc'h et al., *Astrophys. J.* **632**, 169 (2005)
- C. Ledoux, P.M. Vreeswijk, A. Smette, A.J. Fox, P. Petitjean, S.L. Ellison, J.P.U. Fynbo, S. Savaglio, *Astron. Astrophys.* **506**, 661 (2009)
- C. Leitherer, D. Schaerer, J.D. Goldader, R.M.G. Delgado, C. Robert, D.F. Kune, D.F. de Mello, D. Devost, T.M. Heckman, *Astrophys. J. Suppl. Ser.* **123**, 3 (1999)
- A.K. Leroy et al., *Astron. J.* **137**, 4670 (2009)
- B. Lo Faro, P. Monaco, E. Vanzella, F. Fontanot, L. Silva, S. Cristiani, Faint Lyman-break galaxies as a crucial test for galaxy formation models. *Mon. Not. R. Astron. Soc.* **399**, 827–841 (2009). doi:[10.1111/j.1365-2966.2009.15316.x](https://doi.org/10.1111/j.1365-2966.2009.15316.x)
- G.E. Magdis, E. Daddi, M. Sargent et al., *Astrophys. J. Lett.* **758**, L9 (2012a)
- G.E. Magdis, E. Daddi, M. Béthermin et al., [arXiv:1210.1035](https://arxiv.org/abs/1210.1035) (2012b)
- B. Magnelli, D. Elbaz, R.R. Chary et al., *Astron. Astrophys.* **496**, 57 (2009)

- R. Maiolino, P. Cox, P. Caselli, A. Beelen, F. Bertoldi, C.L. Carilli, M.J. Kaufman, K.M. Menten, et al., First detection of [CII]158 μm at high redshift: vigorous star formation in the early universe. *Astron. Astrophys.* **440**, 51–54 (2005). doi:[10.1051/0004-6361:200500165](https://doi.org/10.1051/0004-6361:200500165)
- R. Maiolino, T. Nagao, A. Grazian, F. Cocchia, A. Marconi, F. Mannucci, A. Cimatti, A. Pipino, S. Ballero, F. Calara, C. Chiappini, A. Fontana, G.L. Granato, G. Matteucci, G. Pastorini, L. Pentericci, G. Risaliti, M. Salvati, L. Silva, *Astron. Astrophys.* **488**, 463 (2008)
- F. Mannucci, G. Cresci, R. Maiolino, A. Marconi, A. Gnerucci, *Mon. Not. R. Astron. Soc.* **408**, 2115 (2010)
- C. Maraston, *Mon. Not. R. Astron. Soc.* **362**, 799 (2005)
- D. Marchesini, P.G. van Dokkum, N.M. Forster Schreiber, M. Franx, I. Labbe', S. Wuyts, The evolution of the stellar mass function of galaxies from $z = 4.0$ and the first comprehensive analysis of its uncertainties: evidence for mass-dependent evolution. ArXiv e-prints (2008)
- M. Massardi, A. Bonaldi, M. Negrello et al., *Mon. Not. R. Astron. Soc.* **404**, 532 (2010)
- D. Masters, P. McCarthy, B. Siana, M. Malkan, B. Mobasher, H. Atek, A. Henry, C.L. Martin, M. Rafelski, N.P. Hathi, C. Scarlata, N.R. Ross, A.J. Bunker, G. Blanc, A.G. Bedregal, A. Domínguez, J. Colbert, H. Teplitz, A. Dressler, *Astrophys. J.* **785**, 153 (2014)
- I.S. McLean, C.C. Steidel, H.W. Epps, N. Konidaris, K.Y. Matthews, S. Adkins, T. Aliado, G. Brims, J.M. Canfield, J.L. Cromer, J. Fucik, K. Kulas, G. Mace, K. Magnone, H. Rodriguez, G. Rudie, R. Trainor, E. Wang, B. Weber, J. Weiss, in *Status of the Dark Energy Survey Camera (DECam) Project*. Society of Photo-Optical Instrumentation Engineers (SPIE) Conference Series, vol. 8446 (2012)
- G.R. Meurer, T.M. Heckman, D. Calzetti, *Astrophys. J.* **521**, 64 (1999)
- A.L. Muratov, D. Kereš, C.-A. Faucher-Giguère, P.F. Hopkins, E. Quataert, N. Murray, Gusty, gaseous flows of FIRE: galactic winds in cosmological simulations with explicit stellar feedback. *Mon. Not. R. Astron. Soc.* **454**, 2691–2713 (2015). doi:[10.1093/mnras/stv2126](https://doi.org/10.1093/mnras/stv2126)
- K. Nagamine, V. Springel, L. Hernquist, M. Machacek, Photometric properties of Lyman-break galaxies at $z = 3$ in cosmological SPH simulations. *Mon. Not. R. Astron. Soc.* **350**, 385–395 (2004). doi:[10.1111/j.1365-2966.2004.07664.x](https://doi.org/10.1111/j.1365-2966.2004.07664.x)
- K. Nagamine, J. Choi, H. Yajima, Effects of ultraviolet background and local stellar radiation on the H I column density distribution. *Astrophys. J. Lett.* **725**, 219–222 (2010). doi:[10.1088/2041-8205/725/L219](https://doi.org/10.1088/2041-8205/725/L219)
- C. Night, K. Nagamine, V. Springel, L. Hernquist, Lyman break galaxies at $z = 4-6$ in cosmological smoothed particle hydrodynamics simulations. *Mon. Not. R. Astron. Soc.* **366**, 705–716 (2006). doi:[10.1111/j.1365-2966.2005.09730.x](https://doi.org/10.1111/j.1365-2966.2005.09730.x)
- K.G. Noeske, B.J. Weiner, S.M. Faber, C. Papovich, D.C. Koo, R.S. Somerville, K. Bundy, C.J. Conselice, J.A. Newman, D. Schiminovich, E. Le Flo'c'h, A.L. Coil, G.H. Rieke, J.M. Lotz, J.R. Primack, P. Barmby, M.C. Cooper, M. Davis, R.S. Ellis, G.G. Fazio, P. Guhathakurta, J. Huang, S.A. Kassin, D.C. Martin, A.C. Phillips, R.M. Rich, T.A. Small, C.N.A. Willmer, G. Wilson, *Astrophys. J. Lett.* **660**, L43 (2007)
- D. Obreschkow, S. Rawlings, *Mon. Not. R. Astron. Soc.* **394**, 1857 (2009a)
- D. Obreschkow, S. Rawlings, *Astrophys. J. Lett.* **696**, L129 (2009b)
- M. Onodera et al., *Astrophys. J.* **822**, 42 (2016)
- R.A. Overzier, T.M. Heckman, J. Wang, L. Armus, V. Buat, J. Howell, G. Meurer, M. Seibert, B. Siana, A. Basu-Zych, S. Charlot, T.S. Gonçalves, D.C. Martin, J.D. Neill, R.M. Rich, S. Salim, D. Schiminovich, *Astrophys. J. Lett.* **726**, L7 (2011)
- J.-P. Paardekooper, F.I. Pelupessy, G. Altay, C.J.H. Kruip, The escape of ionising radiation from high-redshift dwarf galaxies. *Astron. Astrophys.* **530**, 87 (2011). doi:[10.1051/0004-6361/201116841](https://doi.org/10.1051/0004-6361/201116841)
- D.A. Perley, A.J. Levan, N.R. Tanvir, S.B. Cenko et al., *Astrophys. J.* **778**, 128 (2013)
- M. Pettini, S.A. Rix, C.C. Steidel, K.L. Adelberger, M.P. Hunt, A.E. Shapley, *Astrophys. J.* **569**, 742 (2002)
- Planck Collaboration, P.A.R. Ade, N. Aghanim, M. Arnaud, M. Ashdown, J. Aumont, C. Baccigalupi, A.J. Banday, R.B. Barreiro, J.G. Bartlett et al., Planck 2015 results. XIII. Cosmological parameters. ArXiv e-prints (2015)
- P. Ranalli, A. Comastri, G. Setti, *Astron. Astrophys.* **399**, 39 (2003)
- A.O. Razoumov, J. Sommer-Larsen, Ionizing radiation from $z = 4-10$ galaxies. *Astrophys. J.* **710**, 1239–1246 (2010). doi:[10.1088/0004-637X/710/2/1239](https://doi.org/10.1088/0004-637X/710/2/1239)
- N.A. Reddy, C.C. Steidel, A steep faint-end slope of the UV luminosity function at $z \sim 2-3$: implications for the global stellar mass density and star formation in low-mass halos. *Astrophys. J.* **692**, 778–803 (2009). doi:[10.1088/0004-637X/692/1/778](https://doi.org/10.1088/0004-637X/692/1/778)
- N.A. Reddy, C.C. Steidel, D. Fadda, L. Yan, M. Pettini, A.E. Shapley, D.K. Erb, K.L. Adelberger, *Astrophys. J.* **644**, 792 (2006)
- N.A. Reddy, D.K. Erb, M. Pettini, C.C. Steidel, A.E. Shapley, *Astrophys. J.* **712**, 1070 (2010)
- N. Reddy, M. Dickinson, D. Elbaz, G. Morrison, M. Giavalisco, R. Ivison, C. Papovich, D. Scott, V. Buat, D. Burgarella, V. Charmandaris, E. Daddi, G. Magdis, E. Murphy, B. Altieri, H. Aussel, H. Dannerbauer, K. Dasyra, H.S. Hwang, J. Kartaltepe, R. Leiton, B. Magnelli, P. Popesso, *Astrophys. J.* **744**, 154 (2012a)

- N.A. Reddy, M. Pettini, C.C. Steidel, A.E. Shapley, D.K. Erb, D.R. Law, *Astrophys. J.* **754**, 25 (2012b)
- N.A. Reddy, M. Kriek, A.E. Shapley, W.R. Freeman, B. Siana, A.L. Coil, B. Mobasher, S.H. Price, R.L. Sanders, I. Shivaiei *ArXiv e-prints* (2015)
- G. Rodighiero, E. Daddi, I. Baronchelli, A. Cimatti, A. Renzini, H. Aussel, P. Popesso, D. Lutz, P. Andreani, S. Berta, A. Cava, D. Elbaz, A. Feltre, A. Fontana, N.M. Förster Schreiber, A. Franceschini, R. Genzel, A. Grazian, C. Gruppioni, O. Ilbert, E. Le Floch, G. Magdis, M. Magliocchetti, B. Magnelli, R. Maiolino, H. McCracken, R. Nordon, A. Poglitsch, P. Santini, F. Pozzi, L. Riguccini, L.J. Tacconi, S. Wuyts, G. Zamorani, *Astrophys. J. Lett.* **739**, L40 (2011)
- E. Romano-Díaz, J.-H. Choi, I. Shlosman, M. Trenti, *Astrophys. J.* **738**, L19 (2011)
- W. Rujopakarn, G.H. Rieke, D.J. Eisenstein, S. Juneau, *Astrophys. J.* **726**, 93 (2011)
- A. Saintonge et al., *Mon. Not. R. Astron. Soc.* **415**, 32 (2011)
- F. Salmi, E. Daddi, D. Elbaz et al., *Astrophys. J. Lett.* **754**, L14 (2012)
- D.B. Sanders, I.F. Mirabel, *Annu. Rev. Astron. Astrophys.* **34**, 749 (1996)
- R.L. Sanders, A.E. Shapley, M. Kriek, N.A. Reddy, W.R. Freeman, A.L. Coil, B. Siana, B. Mobasher, I. Shivaiei, S.H. Price, L. de Groot, *Astrophys. J.* **799**, 138 (2015)
- M.T. Sargent, M. Béthermin, E. Daddi, D. Elbaz, *Astrophys. J. Lett.* **747**, L31 (2012)
- M.T. Sargent et al., *Astrophys. J.* **793**, 19 (2014)
- S. Savaglio, K. Glazebrook, D. Le Borgne, S. Juneau, R.G. Abraham, H.-W. Chen, D. Crampton, P.J. McCarthy, R.G. Carlberg, R.O. Marzke, K. Roth, I. Jørgensen, R. Murowinski, *Astrophys. J.* **635**, 260 (2005)
- J. Schaye, C. Dalla Vecchia, On the relation between the Schmidt and Kennicutt-Schmidt star formation laws and its implications for numerical simulations. *Mon. Not. R. Astron. Soc.* **383**, 1210–1222 (2008). doi:[10.1111/j.1365-2966.2007.12639.x](https://doi.org/10.1111/j.1365-2966.2007.12639.x)
- J. Schaye, R.A. Crain, R.G. Bower, M. Furlong, M. Schaller, T. Theuns, C. Dalla Vecchia, C.S. Frenk, I.G. McCarthy, J.C. Helly, A. Jenkins, Y.M. Rosas-Guevara, S.D.M. White, M. Baes, C.M. Booth, P. Camps, J.F. Navarro, Y. Qu, A. Rahmati, T. Sawala, P.A. Thomas, J. Trayford, The EAGLE project: simulating the evolution and assembly of galaxies and their environments. *Mon. Not. R. Astron. Soc.* **446**, 521–554 (2015). doi:[10.1093/mnras/stu2058](https://doi.org/10.1093/mnras/stu2058)
- A. Schruha, A.K. Leroy, F. Walter et al., *Astron. J.* **143**, 138 (2012)
- M. Seibert, D.C. Martin, T.M. Heckman, V. Buat, C. Hoopes, T. Barlow, L. Bianchi, Y.-I. Byun, J. Donas, K. Forster, P.G. Friedman, P. Jelinsky, Y.-W. Lee, B.F. Madore, R. Malina, B. Milliard, P. Morrissey, S. Neff, R.M. Rich, D. Schiminovich, O. Siegmund, T. Small, A.S. Szalay, B. Welsh, T.K. Wyder, *Astrophys. J. Lett.* **619**, L55 (2005)
- A.E. Shapley, *Annu. Rev. Astron. Astrophys.* **49**, 525 (2011)
- A.E. Shapley, N.A. Reddy, M. Kriek, W.R. Freeman, R.L. Sanders, B. Siana, A.L. Coil, B. Mobasher, I. Shivaiei, S.H. Price, L. de Groot, *Astrophys. J.* **801**, 88 (2015)
- I. Shivaiei, N.A. Reddy, A.E. Shapley, M. Kriek, B. Siana, B. Mobasher, A.L. Coil, W.R. Freeman, R. Sanders, S.H. Price, L. de Groot, M. Azadi *ArXiv e-prints* (2015)
- R. Smit, R.J. Bouwens, M. Franx, G.D. Illingworth, I. Labbé, P.A. Oesch, P.G. van Dokkum, The star formation rate function for redshift $z \sim 4-7$ galaxies: evidence for a uniform buildup of star-forming galaxies during the first 3 Gyr of cosmic time. *Astrophys. J.* **756**, 14 (2012). doi:[10.1088/0004-637X/756/1/14](https://doi.org/10.1088/0004-637X/756/1/14)
- B.M. Smith, R.A. Windhorst, R.A. Jansen, S.H. Cohen, L. Jiang, M. Dijkstra, A.M. Koekemoer, R. Bielby, A.K. Inoue, J.W. MacKenty, R.W. O'Connell, J.I. Silk, Hubble Space Telescope Wide Field Camera 3 observations of escaping Lyman continuum radiation from galaxies and weak AGN at redshifts $z \sim 2.3-5$. *ArXiv e-prints* (2016)
- P.M. Solomon, D. Downes, S.J.E. Radford, J.W. Barrett, *Astrophys. J.* **478**, 144 (1997)
- M. Sparre, O.E. Hartoog, T. Krühler, J.P.U. Fynbo, D.J. Watson, K. Wiersema, V. D'Elia, T. Zafar, P.M.J. Afonso, S. Covino, A. de Ugarte Postigo, H. Flores, P. Goldoni, J. Greiner, J. Hjorth, P. Jakobsson, L. Kaper, S. Klose, A.J. Levan, D. Malesani, B. Milvang-Jensen, M. Nardini, S. Piranomonte, J. Sollerman, R. Sánchez-Ramírez, S. Schulze, N.R. Tanvir, S.D. Vergani, R.A.M.J. Wijers, *Astrophys. J.* **785**, 150 (2014)
- J.S. Spilker et al., *Astrophys. J.* **785**, 149 (2014)
- V. Springel, The cosmological simulation code GADGET-2. *Mon. Not. R. Astron. Soc.* **364**, 1105–1134 (2005). doi:[10.1111/j.1365-2966.2005.09655.x](https://doi.org/10.1111/j.1365-2966.2005.09655.x)
- V. Springel, L. Hernquist, Cosmological smoothed particle hydrodynamics simulations: a hybrid multiphase model for star formation. *Mon. Not. R. Astron. Soc.* **339**, 289–311 (2003). doi:[10.1046/j.1365-8711.2003.06206.x](https://doi.org/10.1046/j.1365-8711.2003.06206.x)
- C.C. Steidel, G.C. Rudie, A.L. Strom, M. Pettini, N.A. Reddy, A.E. Shapley, R.F. Trainor, D.K. Erb, M.L. Turner, N.P. Konidaris, K.R. Kulas, G. Mace, K. Matthews, I.S. McLean *ArXiv e-prints* (2014)
- L.J. Tacconi et al., *Nature* **463**, 781 (2010)
- L.J. Tacconi et al., *Astrophys. J.* **768**, 74 (2013)

- Q. Tan et al., *Astrophys. J.* **776**, L24 (2013)
- Q. Tan et al., *Astron. Astrophys.* **569**, A98 (2014)
- N.R. Tanvir, D.B. Fox, A.J. Levan, E. Berger, K. Wiersema, J.P.U. Fynbo, A. Cucchiara, T. Krühler, N. Gehrels, J.S. Bloom, J. Greiner, P.A. Evans, E. Rol, F. Olivares, J. Hjorth, P. Jakobsson, J. Farihi, R. Willingale, R.L.C. Starling, S.B. Cenko, D. Perley, J.R. Maund, J. Duke, R.A.M.J. Wijers, A.J. Adamson, A. Allan, M.N. Bremer, D.N. Burrows, A.J. Castro-Tirado, B. Cavanagh, A. de Ugarte Postigo, M.A. Dopita, T.A. Fatkhullin, A.S. Fruchter, R.J. Foley, J. Gorosabel, J. Kennea, T. Kerr, S. Klöse, H.A. Krimm, V.N. Komarova, S.R. Kulkarni, A.S. Moskvitin, C.G. Mundell, T. Naylor, K. Page, B.E. Penprase, M. Perri, P. Podsiadlowski, K. Roth, R.E. Rutledge, T. Sakamoto, P. Schady, B.P. Schmidt, A.M. Soderberg, J. Sollerman, A.W. Stephens, G. Stratta, T.N. Ukwatta, D. Watson, E. Westra, T. Wold, C. Wolf, A γ -ray burst at a redshift of $z \sim 8.2$. *Nature* **461**, 1254–1257 (2009). doi:[10.1038/nature08459](https://doi.org/10.1038/nature08459)
- M. Tegmark, M.A. Strauss, M.R. Blanton, K. Abazajian, S. Dodelson, H. Sandvik, X. Wang, D.H. Weinberg, I. Zehavi, N.A. Bahcall, F. Hoyle, D. Schlegel, R. Scoccimarro, M.S. Vogeley, A. Berlind, T. Budavari, A. Connolly, D.J. Eisenstein, D. Finkbeiner, J.A. Frieman, J.E. Gunn, L. Hui, B. Jain, D. Johnston, S. Kent, H. Lin, R. Nakajima, R.C. Nichol, J.P. Ostriker, A. Pope, R. Scranton, U. Seljak, R.K. Sheth, A. Stebbins, A.S. Szalay, I. Szapudi, Y. Xu, J. Annis, J. Brinkmann, S. Burles, F.J. Castander, I. Csabai, J. Loveday, M. Doi, M. Fukugita, B. Gillespie, G. Hennessy, D.W. Hogg, Ž. Ivezić, G.R. Knapp, D.Q. Lamb, B.C. Lee, R.H. Lupton, T.A. McKay, P. Kunszt, J.A. Munn, L. O’Connell, J. Peoples, J.R. Pier, M. Richmond, C. Rockosi, C. Stoughton, D.L. Tucker, D.E. vanden Berk, B. Yanny, D.G. York, Cosmological parameters from SDSS and WMAP. *Phys. Rev. D* **69**(10), 103501 (2004). doi:[10.1103/PhysRevD.69.103501](https://doi.org/10.1103/PhysRevD.69.103501)
- R. Thompson, K. Nagamine, J. Jaacks, J.-H. Choi, Molecular hydrogen regulated star formation in cosmological smoothed particle hydrodynamics simulations. *Astrophys. J.* **780**, 145 (2014). doi:[10.1088/0004-637X/780/2/145](https://doi.org/10.1088/0004-637X/780/2/145)
- C.A. Tremonti, T.M. Heckman, G. Kauffmann, J. Brinchmann, S. Charlot, S.D.M. White, M. Seibert, E.W. Peng, D.J. Schlegel, A. Uomoto, M. Fukugita, J. Brinkmann, *Astrophys. J.* **613**, 898 (2004)
- P. Troncoso, R. Maiolino, V. Sommariva, G. Cresci, F. Mannucci, A. Marconi, M. Neghetti, A. Grazian, A. Cimatti, A. Fontana, T. Nagao, L. Pentericci, *Astron. Astrophys.* **563**, A58 (2014)
- M. Vogelsberger, S. Genel, V. Springel, P. Torrey, D. Sijacki, D. Xu, G. Snyder, D. Nelson, L. Hernquist, Introducing the Illustris Project: simulating the coevolution of dark and visible matter in the Universe. *Mon. Not. R. Astron. Soc.* **444**, 1518–1547 (2014). doi:[10.1093/mnras/stu1536](https://doi.org/10.1093/mnras/stu1536)
- B.J. Weiner, A.L. Coil, J.X. Prochaska, J.A. Newman, M.C. Cooper, K. Bundy, C.J. Conselice, A.A. Dutton, et al., Ubiquitous Outflows in DEEP2 spectra of star-forming galaxies at $z = 1.4$. *Astrophys. J.* **692**, 187–211 (2009). doi:[10.1088/0004-637X/692/1/187](https://doi.org/10.1088/0004-637X/692/1/187)
- K.E. Whitaker, M. Franx, J. Leja, P.G. van Dokkum, A. Henry, R.E. Skelton, M. Fumagalli, I.G. Momcheva, G.B. Brammer, I. Labbé, E.J. Nelson, J.R. Rigby, *Astrophys. J.* **795**, 104 (2014)
- S.M. Wilkins, A. Bunker, W. Coulton, R. Croft, T.D. Matteo, N. Khandai, Y. Feng, *Mon. Not. R. Astron. Soc.* **430**, 2885 (2013)
- J.H. Wise, R. Cen, Ionizing photon escape fractions from high-redshift dwarf galaxies. *Astrophys. J.* **693**, 984–999 (2009). doi:[10.1088/0004-637X/693/1/984](https://doi.org/10.1088/0004-637X/693/1/984)
- S. Wuyts, N.M. Förster Schreiber, A. van der Wel et al., *Astrophys. J.* **742**, 96 (2011)
- J.S.B. Wyithe, A.M. Hopkins, M.D. Kistler, H. Yüksel, J.F. Beacom, Determining the escape fraction of ionizing photons during reionization with the GRB-derived star formation rate. *Mon. Not. R. Astron. Soc.* **401**, 2561–2571 (2010). doi:[10.1111/j.1365-2966.2009.15834.x](https://doi.org/10.1111/j.1365-2966.2009.15834.x)
- H. Yajima, J.-H. Choi, K. Nagamine, Escape fraction of ionizing photons from high-redshift galaxies in cosmological SPH simulations. *Mon. Not. R. Astron. Soc.* **412**, 411–422 (2011). doi:[10.1111/j.1365-2966.2010.17920.x](https://doi.org/10.1111/j.1365-2966.2010.17920.x)
- H. Yajima, I. Shlosman, E. Romano-Díaz, K. Nagamine, Observational properties of simulated galaxies in overdense and average regions at redshifts $z \sim 6$ –12. *Mon. Not. R. Astron. Soc.* **451**, 418–432 (2015). doi:[10.1093/mnras/stv974](https://doi.org/10.1093/mnras/stv974)
- G. Yepes, R. Kates, A. Khokhlov, A. Klypin, Hydrodynamical simulations of galaxy formation: effects of supernova feedback. *Mon. Not. R. Astron. Soc.* **284**, 235–256 (1997)
- A. Zanella et al., *Nature* **521**, 54 (2015)